N73-21827

PREDICTION OF SHUTTLE VEHICLE DAMPING FROM COMPONENT TEST RESULTS

by
Daniel D. Kana
James F. Unruh

FINAL REPORT

Contract No. NAS8-27569
Control No. 1-1-50-13733 (2F)
SwRI Project No. 02-3131

Prepared for
National Aeronautics and Space Administration
George C. Marshall Space Flight Center
Marshall Space Center, Alabama

March 1973

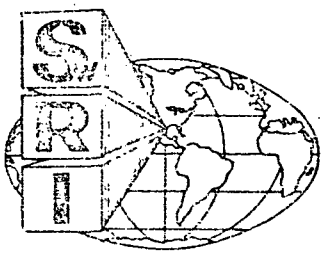

SOUTHWEST RESEARCH INSTITUTE
SAN ANTONIO CORPUS CHRISTI HOUSTON

SOUTHWEST RESEARCH INSTITUTE
Post Office Drawer 28510, 8500 Culebra Road
San Antonio, Texas 78284

PREDICTION OF SHUTTLE VEHICLE DAMPING FROM COMPONENT TEST RESULTS

by
Daniel D. Kana
James F. Unruh

FINAL REPORT

Contract No. NAS8-27569
Control No. 1-1-50-13733 (2F)
SwRI Project No. 02-3131

Prepared for
National Aeronautics and Space Administration
George C. Marshall Space Flight Center
Marshall Space Center, Alabama

March 1973

Approved:

H. Norman Abramson,
Technical Vice President

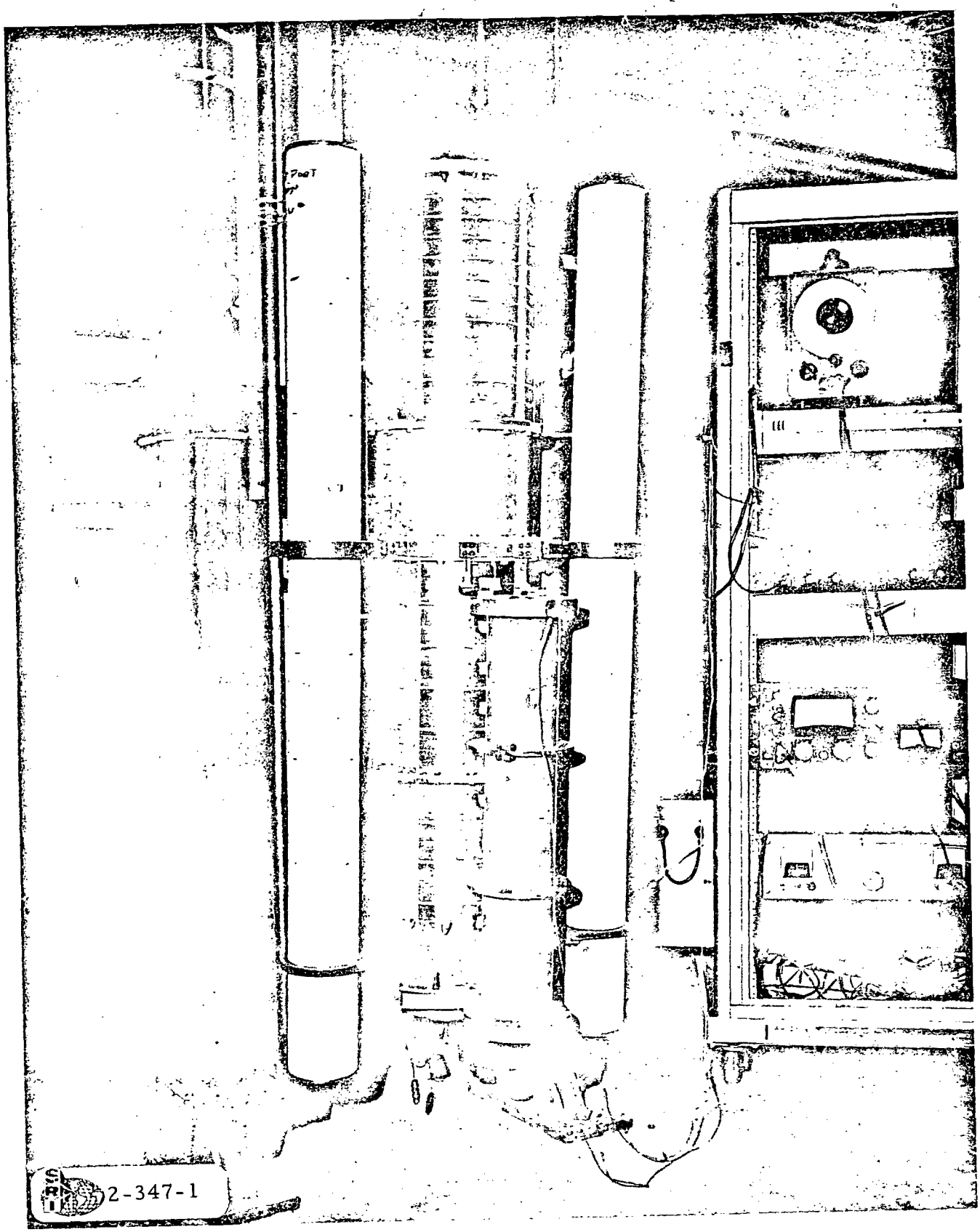

Photograph of Shuttle Model

ABSTRACT

The results of this program have demonstrated the validity of a dissipative energy approach for predicting the damping of a four-component Space Shuttle model by means of modal parameters obtained from tests of the individual components. A relationship between modal damping energy per cycle and peak strain (or kinetic) energy is first determined empirically from test data for each component. Undamped analytical models of each component are also developed, and combined into a System model from which are obtained modal kinetic (or strain) energies for its respective modes. These data are then used with the empirical damping curves to apportion the proper amount of damping energy to each component in a combined System mode, and thereby allow a prediction of damping ratio. Some discrepancies in results are noted to occur because of incomplete modeling of connecting link mechanisms and anomalies in modal responses.

TABLE OF CONTENTS

LIST OF ILLUSTRATIONS

LIST OF TABLES

I. INTRODUCTION

The complexity and size of the Space Shuttle vehicle renders the task of full scale System dynamic testing extremely unfeasible. Nevertheless, System modal properties, including damping, must be acquired by some means for accurate prediction of dynamic response. It is also recognized that full scale testing of Shuttle-type substructures is entirely feasible, and in fact, would be quite similar to previous testing of Saturn and other vehicles. Therefore, for some months, a technique has been sought for prediction of System properties from design parameters, as well as those measured on full scale tests of individual components. Currently-available analytical methods for synthesis of System mass and stiffness properties have been found to be entirely adequate for prediction of free natural modes[1*]. However, synthesis of damping and development of techniques for its prediction have been found to be very much in an infant state.

In the earlier phase of this program, an energy approach[2] was developed for correlating modal damping data which were obtained on components of a simple parallel stage Shuttle model, and for further combination of those data into a prediction of modal damping for the combined System. Comparisons of predicted and measured data showed extremely good overall agreement for the relatively simple model. Therefore, it became appropriate to consider whether this energy approach was valid when applied to a more representative, four-component Shuttle model. The purpose of this report is to present the results of this further investigation.

In conducting the investigation our objectives can be summarized as follows:

(1) Design a four-component, three-dimensional parallel stage Shuttle model which includes liquids in the Hydrogen/Oxygen (H/O) tank, and which includes built-up construction and component connecting joints that simulate to some degree those envisioned for the base line Shuttle design.

(2) Develop an analytical model for the substructures and combine them into a model for the total System. Predict natural frequencies, modes, modal mass, modal stiffness and kinetic and strain energies from this model.

---

*Superscript numbers indicate references which will be found on page 44.

(3) Perform dynamic tests of the substructures and joints to determine their properties. In particular, determine whether the previously-derived damping energy correlation can be established for components of this design.

(4) Use the previously-developed energy method to predict the modal damping properties for the System.

(5) Perform dynamic tests on the combined System to verify the adequacy of the analytical model and establish the applicability of the damping energy prediction method to this type of model.

In carrying out these objectives, it was recognized that the main emphasis should be on verification of damping prediction methods, rather than verification of free vibration modal analysis techniques. Nevertheless, the latter techniques are inherently required in the subject approach to damping prediction. Further, the combined System model, which has been shown in the Frontispiece, can be imagined to require reasonable facility for free vibration modal analysis alone, even though it is rather rudimentary compared to a full size Shuttle design. Therefore, in the development of the analytical model, free vibration modal analysis of the components was tuned as much as possible to experimental results obtained from the free-free tests on individual components. Further, connecting link stiffness properties were modeled from results of intermediate tests in which the components were mounted against a rigid wall. In view of all this, we still wish to emphasize that no restrictions have been inherently included in the damping prediction method as a result of this procedure.

II. DESCRIPTION OF PHYSICAL MODEL

A photograph of the combined System model has been shown in the Frontispiece. Some general dimensions and details are further given in the three-view drawing of Figure 1. The H/O component basically consists of two 0.005-in. wall stainless steel liquid propellant tanks, each having an ellipsoidal bulkhead, and joined together through an aluminum skirt section. The upper tank and skirt and the aluminum bulkheads have been used before in previous studies[3]. The lower tank is fabricated in two sections that are joined together with a ring flange. Ethylene glycol is used as a model propellant in both tanks. Ring and wire circumferential stiffners are provided on both tanks to subdue localized shell mode response and thereby not obscure overall bending and longitudinal response.

The Orbiter and two Solid Rocket Motors (SRM's) are made of 1/4-in. wall polyvinyl chloride tubing. This material was chosen because it demonstrated modal damping of the order of 1% critical. It was felt that values in this range were desirable to allow reasonable measurement accuracy. Values from the all-metal H/O tank will be seen to be considerably lower. These components also were fitted with solid steel end and mounting rings to emphasize overall bending, longitudinal and torsional responses.

Mounting points for the several components were provided on a solid 1-in. thick steel disk and annular ring which formed part of the H/O tank. The disk forms the forward mounting point and attachment for a simulated free-free suspension (see the Frontispiece). The steel ring formed the aft mounting point.

Details of the mounting springs and pins are shown in Figure 2. The forward Orbiter and aft SRM joints consist of the steel double flexures shown in Figure 2a. These flexures are designed to be significantly stiff in the vertical direction for each respective component, and very compliant (essentially only a guide) in the longitudinal direction. The aft Orbiter and forward SRM joints consist of the three-dimensional pin arrangement shown in detail in Figure 2b. The pins themselves are designed from Bendix Flexure Pivots. Although it was hoped that this joint would act essentially as a 3-D pin joint, it was found through later tests that significant compliance was present in all three translational dimensions, and spring constants had to be assigned for these joints in the analytical model. Likewise, all joints were designed to provide very low damping. However, it was later found that this parameter was not insignificant for the lower modes, and some accounting for it had to be provided.

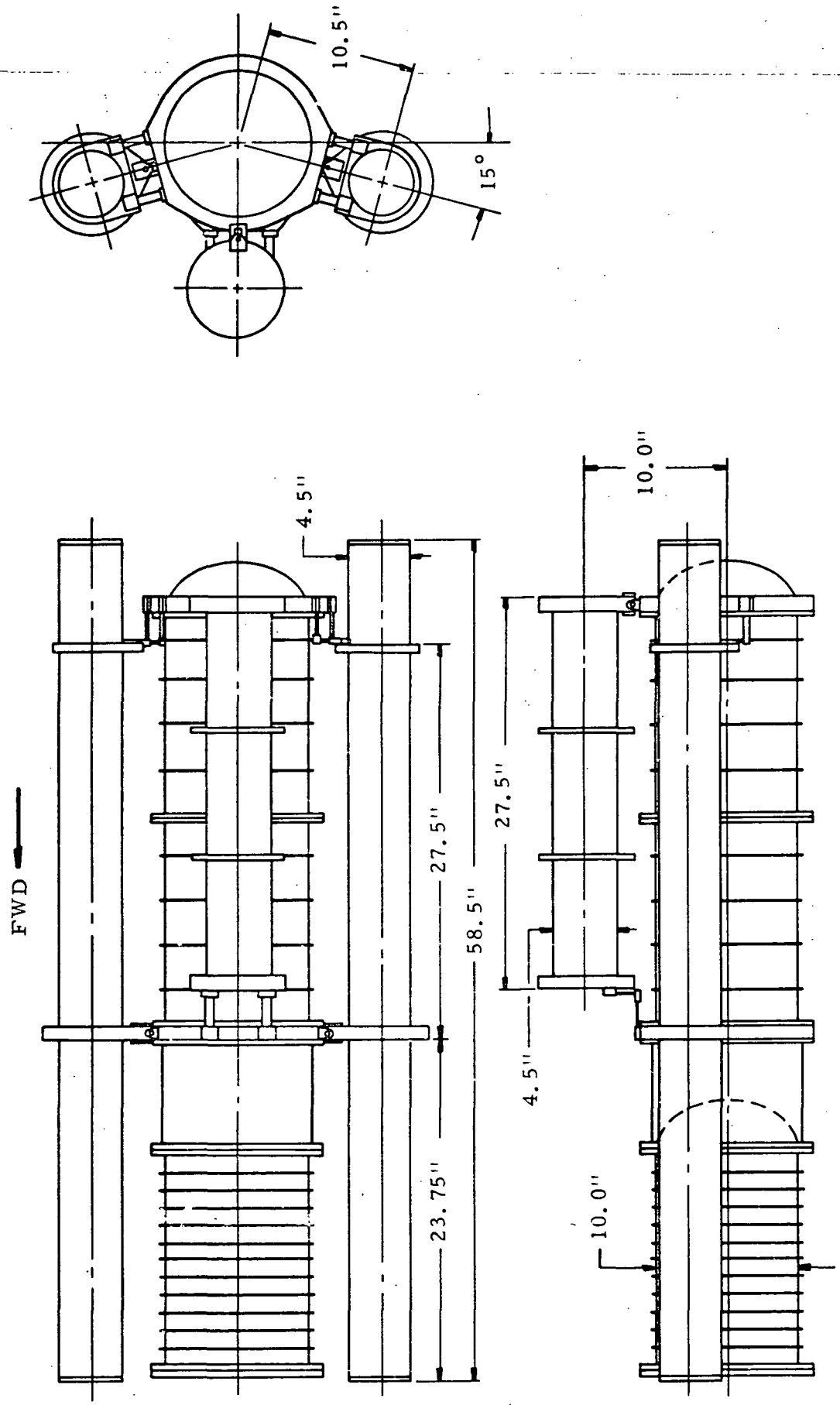

Figure 1. General Design of Shuttle Model

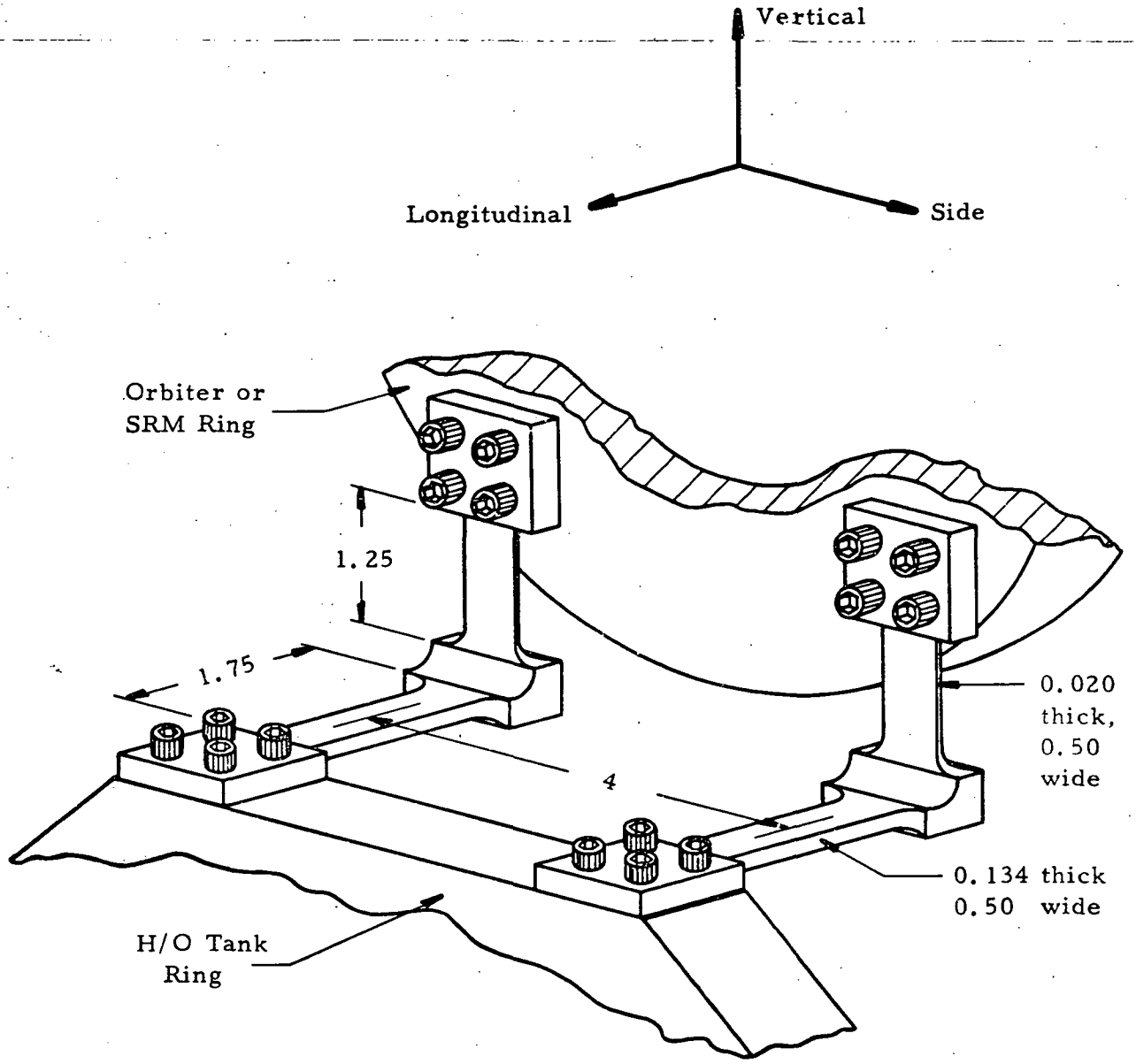

Figure 2a. Detail of Connecting Links-Double Flexures

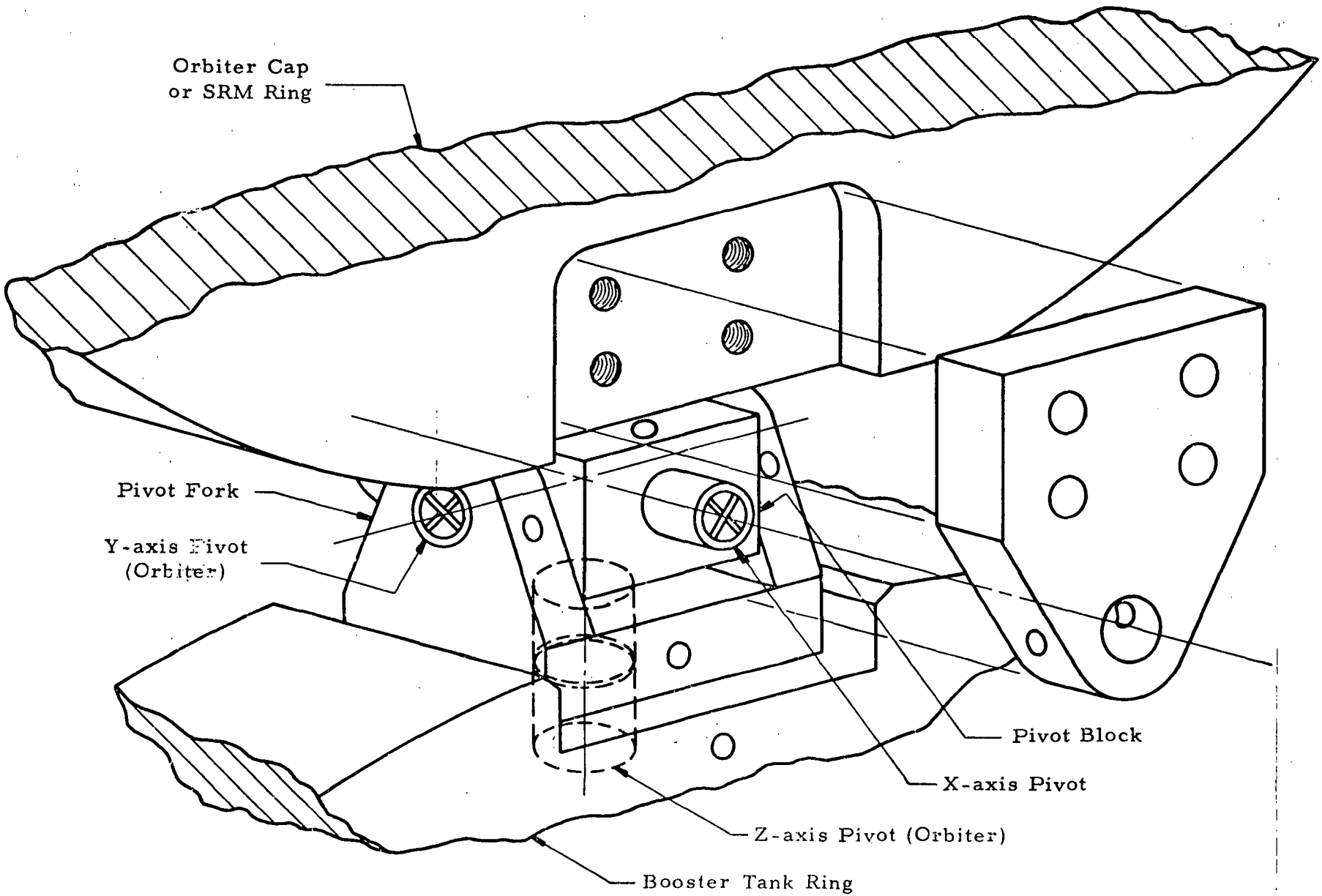

Figure 2b. Detail of Connecting Links - Pin Joints

From the above description it can be seen that the combined model was designed to experience modes which include rigid body motion of the components against the mounting joints at low frequencies, various combinations of bending, torsion, and longitudinal response combined with spring motion at intermediate frequencies, and all three of the latter without significant spring motion at higher frequencies. The general range for frequencies of given types of modes was designed to be ratioed to corresponding modes for the baseline Shuttle vehicle design, where possible. In this regard, however, liquid slosh modes were not brought into a range of significant coupling. Finally, it should be recognized that no external damping was applied to the System. Energy dissipation was confined to internal damping of the individual components and that of the six connecting links.

III. ANALYTICAL MODELING

A. Free-Free Component Analysis

The structural dynamics representation of the free-free components employed finite element beam models for bending, torsional and longitudinal stiffness characteristics with the exception being a simple translational spring representation for the longitudinal H/O Tank. In general, the mass properties of the components were lumped at the structural nodes. Where applicable, the effects of transverse shear and rotatory inertia were taken into account.

Due to the symmetry of the Orbiter and SRM components, the bending models in mutually perpendicular axes were made identical. The Orbiter free-free model consisted of 14 degrees of freedom in the bending model and 7 degrees of freedom in both the torsion model and longitudinal model. Likewise, the SRM's were modeled with 18 bending, 9 torsional, and 9 longitudinal degrees of freedom. A single SRM model was used to represent the Port or Starboard SRM components.

Preliminary analysis of the slosh response of the nearly full H/O Tank showed the slosh frequencies to be much lower (around 2.0 Hz) than the expected system responses and therefore it was felt that only negligible coupling would occur. For this reason, the H/O Tank slosh model was not used in the investigation. Due to the welded seam construction as well as some localized buckling of the tank skins, two bending models of the H/O Tank in mutually perpendicular directions were necessary. The H/O Tank was modeled as two substructures with the upper tank and skirt being one substructure and the lower tank being the second. Twelve bending degrees of freedom were used in each of the substructures. In the torsional model of the H/O Tank, 4 degrees of freedom were used in the upper tank and skirt while 5 degrees of freedom were used in the lower tank.

The longitudinal model of the H/O upper tank and skirt were available from previous work[3] and consisted of 1 liquid and 3 structural degrees of freedom. The lower tank was modeled with 2 liquid and 2 structural degrees of freedom using the longitudinal mass-spring model of Glaser[4]. The effects of the ellipsoidal bulkheads were indirectly taken into account when the models were tuned to the experimental results.

Free-free eigenvalue-eigenvector results on all the components were obtained from constrained substructure modes[5]. Each component was constrained at its attach points to the coupled structure and a free-free analysis was performed with constrained modes. The models were

tuned to the free-free experimental frequencies, the results of which are given in a later section.

B. Spring-Pin Component Analysis

The spring supports were modeled using equivalent translational and rotational springs. Due to the compliance in the ball joint support, additional translational springs at the ball joints were also necessary for accurate modeling. Due to the symmetry of the supports, both the Orbiter and SRM components were modeled wherein only vertical bending and longitudinal motion coupled as well as side bending and torsional motion. For the component motion designation used herein, see Figure 3.

To tune the spring supports, the Orbiter and SRM components were constrained to a wall at their attach points to the H/O Tank. Frequency and mode shape information was obtained from which the model spring supports and ball joint compliances were tuned. Comparison of these results are discussed in a later section.

C. Free-Free System Analysis

Due to the symmetry in the model, the free-free coupled system was modeled via a symmetric analysis consisting of rigid body vertical translation, pitch and longitudinal motion and an antisymmetric analysis consisting of rigid body side translation, yaw and roll. Due to the SRM's being located fifteen degrees off the side bending axis, all six degrees of freedom of the SRM's were required in both the symmetric and antisymmetric analyses. In Table I the number of nodal degrees of freedom and the number of retained constrained modes for each substructure component is listed. Coupled system frequencies and mode shapes were obtained using the coupled substructure analysis technique referenced above.

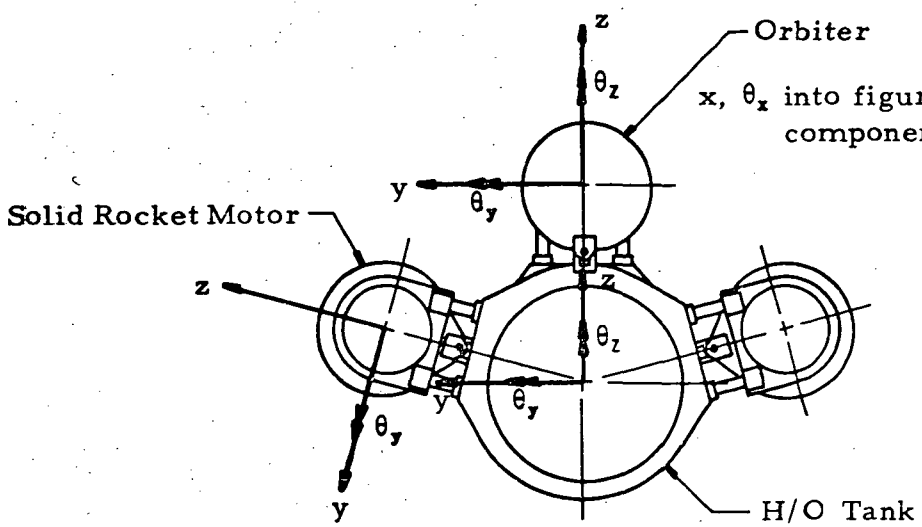

Degrees of Freedom

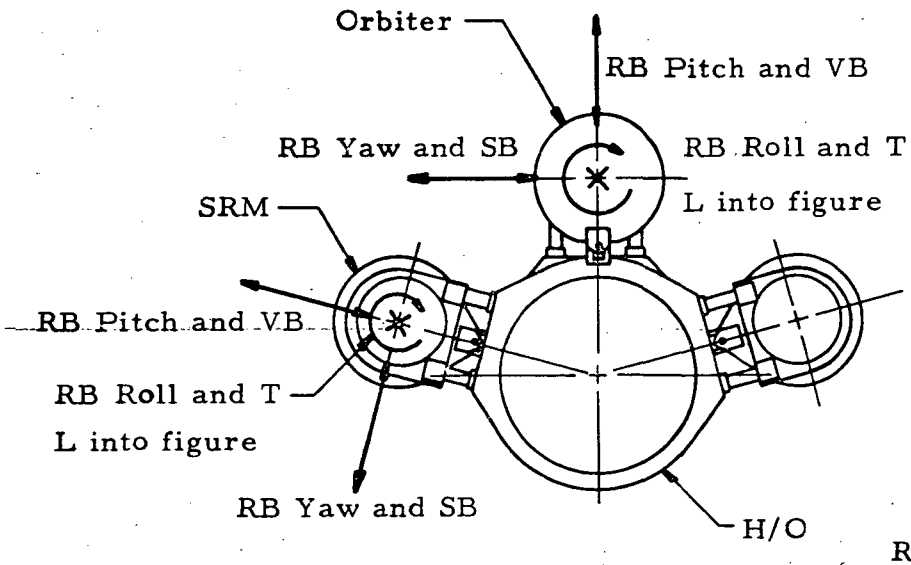

Note: H/O Tank Nomenclature Same as Orbiter

Nomenclature

RB	Rigid Body
L	Longitudinal
T	Torsion
VB	Vertical Bending
SB	Side Bending

Figure 3. Component Motion Designation

TABLE I. COMPONENT DEGREES OF FREEDOM SUMMARY

A. Symmetric Analysis

Component	Allowable Motion	Nodal Degrees of Freedom	Retained Component Modes
Fwd H/O	$x \sim L$	4	3
Aft H/O	$x \sim L$	4	2
Fwd H/O	$z - \theta_y \sim VB$	12	5
Aft H/O	$z - \theta_y \sim VB$	12	7
Orbiter	$x\text{-}z\text{-}\theta_y \sim L\&VB$	26	7
SRM	$x\text{-}z\text{-}\theta_y \sim L\&VB$	32	11
SRM	$y\text{-}\theta_x\text{-}\theta_z \sim SB\&T$	31	11
		121	46

B. Antisymmetric Analysis

Fwd H/O	$\theta_x \sim T$	4	3
Aft H/O	$\theta_x \sim T$	5	3
Fwd H/O	$y - \theta_z \sim SB$	12	5
Aft H/O	$y - \theta_z \sim SB$	12	5
Orbiter	$y\text{-}\theta_x\text{-}\theta_z \sim SB\&T$	25	9
SRM	$x\text{-}z\text{-}\theta_y \sim L\text{-}VB$	32	11
SRM	$y\text{-}\theta_x\text{-}\theta_z \sim SB\text{-}T$	31	11
		121	47

IV. EXPERIMENTAL PROCEDURES

A. Component Tests

The first series of component tests consisted of suspending each individual component on a low frequency suspension which approximated a free-free condition, and performing resonance tests. Mode shapes were qualitatively identified and frequencies noted. At the same time, measurements of damping and modal kinetic energy were measured. Damping was usually determined from free decay records. However, in some cases beating between closely spaced modes necessitated the use of the half-bandwidth technique, and in a few cases precluded any damping measurement at all. Measurement of modal kinetic energy was accomplished indirectly. Actually, dissipated energy per cycle at resonance was determined by measuring input force and displacement. The displacement at the point of maximum modal response on the structure was also measured. Damping energy per cycle $\bar{D}_c$ was then determined for a normalized maximum modal amplitude of one millimeter. Normalized modal kinetic energy $\bar{T}_o$ was then determined from

$$\bar{T}_o = \frac{\bar{D}_c}{4\pi\zeta}$$

where ζ was determined by free decay. It should be noted that this procedure assumes the existence of damping linearity with response amplitude.

In carrying out the above procedure, similar tests were run by excitation along three different perpendicular axes. On the Orbiter and two SRM's it was found that modal properties, including damping, did not vary along the two transverse axes (i.e., the models were symmetrical). However, it was found that significant variations did occur in the H/O Tank model. This apparently resulted because of the seam-welded tank construction, as well as the presence of some localized buckled areas in the lower tank. This problem was handled by postulating different models along the pitch and yaw axes of the H/O Tank. These experiments were conducted only for nearly full liquid levels. Available resources did not allow measurements at other levels. In addition, measurements of pressure at the center of the two bulkheads aided in isolating longitudinal liquid modes. No measurements were made on lateral slosh modes.

A second series of component tests were run with the Orbiter and SRM's each mounted on a rigid wall through their respective

mounting springs and pins. Similar measurements were made as before, except that modal kinetic energies were not determined. These tests served principally as a check on the analytical modeling of the connecting links, and served as an intermediate step for checking the method of damping prediction. However, as will be explained later, undesired vibration of the support structure caused extraneous damping which reduced the value of the latter comparison. This difficulty in no way affected the later System measurements.

B. Connecting Link Tests

Tests to determine damping properties of the connecting links were conducted on the links alone (i.e., not connected to the major components) before the major components were assembled. Double flexures were tested in pairs by means of a simulated mounting which can be described by referring to Figure 2a. The double flexures were mounted on the H/O Tank ring and this ring was clamped to a rigid mounting block. In place of the Orbiter or SRM ring, the other ends of the flexures were joined on a solid steel bar. This bar had dimensions 1/4-in. thick, 1-in. wide, and 5-in. long. Thus, the solid bar acted as a mass cantilevered on the two flexure pivots. This integral structure was resonance tested similar to the major components by excitation in each the vertical and side directions. Excitation in the longitudinal direction was not considered because of the inherent weakness in that direction. Damping ratios and kinetic energies were measured for several modes of this compound structure.

The 3-D pivot was also resonance tested in the vertical direction only. This was accomplished by mounting one side in the H/O ring, and mounting a solid block on the other end of the pivot. Only one mode could be identified in this manner. Testing in the side and longitudinal directions on this joint was not readily possible because of the large compliance in rotation along those axes.

C. System Tests

Procedures for System tests were essentially the same as for component testing, except that no dissipated energy values were measured. This was not necessary for the comparison of predicted and measured damping ratios. Modes and frequencies were qualitatively identified by observing the outputs of accelerometers mounted at various locations. The position of the exciter coil had to be changed several times in order to optimize the response of certain modes. Even so,

a number of the modal responses were either too obscure or beating instabilities between closely spaced modes prevented the acquisition of good data. Likewise, in some cases mixing of symmetric and antisymmetric modes occurred when they were closely spaced. In spite of these difficulties, a variety of numerous modes were identified and data obtained on them.

V. FREE-FREE COMPONENT RESULTS

A. Major Components

Analytical modes and frequencies for the free-free components are presented in Figure 4. Although more modes were determined, we show only those that are significant through a 400 Hz frequency range. The indicated mode identification abbreviations will be used from here on except that the (F), which indicates free test, will be dropped. Note that two frequencies are given for the bending modes of the H/O Tank. This corresponds to the different stiffnesses that were experienced along orthogonal axes, as has been previously described.

A comparison of theoretical and experimental frequencies is given in Table II. Measured damping data is also given for information. By appropriate adjustment of various analytical model stiffness parameters, it can be seen that excellent agreement was achieved in the frequencies. Although the experimental frequencies were essentially identical for the two SRM's, slight variations in damping can be noted.

Damping energy information for the H/O Tank is presented in Figure 5. It should be recognized that modal kinetic and strain energies are equal for such free-free resonances. It is obvious that basically two different damping processes occur, one associated with all types of modes of the structure itself, and one with the longitudinal modes of the liquid. It is not surprising that essentially two different mechanisms would influence damping processes for such modes. This formation of two different correlations was not encountered in the earlier work[2], but can still be readily incorporated into the damping prediction method, as will be shown in the next section. It was gratifying to find that the damping energy data for the built-up component with liquid, did fall into some correlation pattern. This is an absolute requirement for the damping prediction method to be used.

Similar damping energy data is shown in Figure 6 for the Orbiter and two SRM's. Data for all types of modes correlate on the same line when normalized to the same amplitude. In this, torsional mode amplitudes were taken as that at the mean radius of the component tube wall. This is a new discovery that was not included in the earlier work because of a lack of different types of modes in that work. Although the Orbiter geometry is significantly different from the SRM's, it still correlates on the same line. Since their material content is identical, it appears that the material alone that is strained during vibration is what influences the correlation line. Geometry differences and types of modes do not cause a separation in data. This in itself is an extremely important discovery for correlation of damping data from a design point of view.

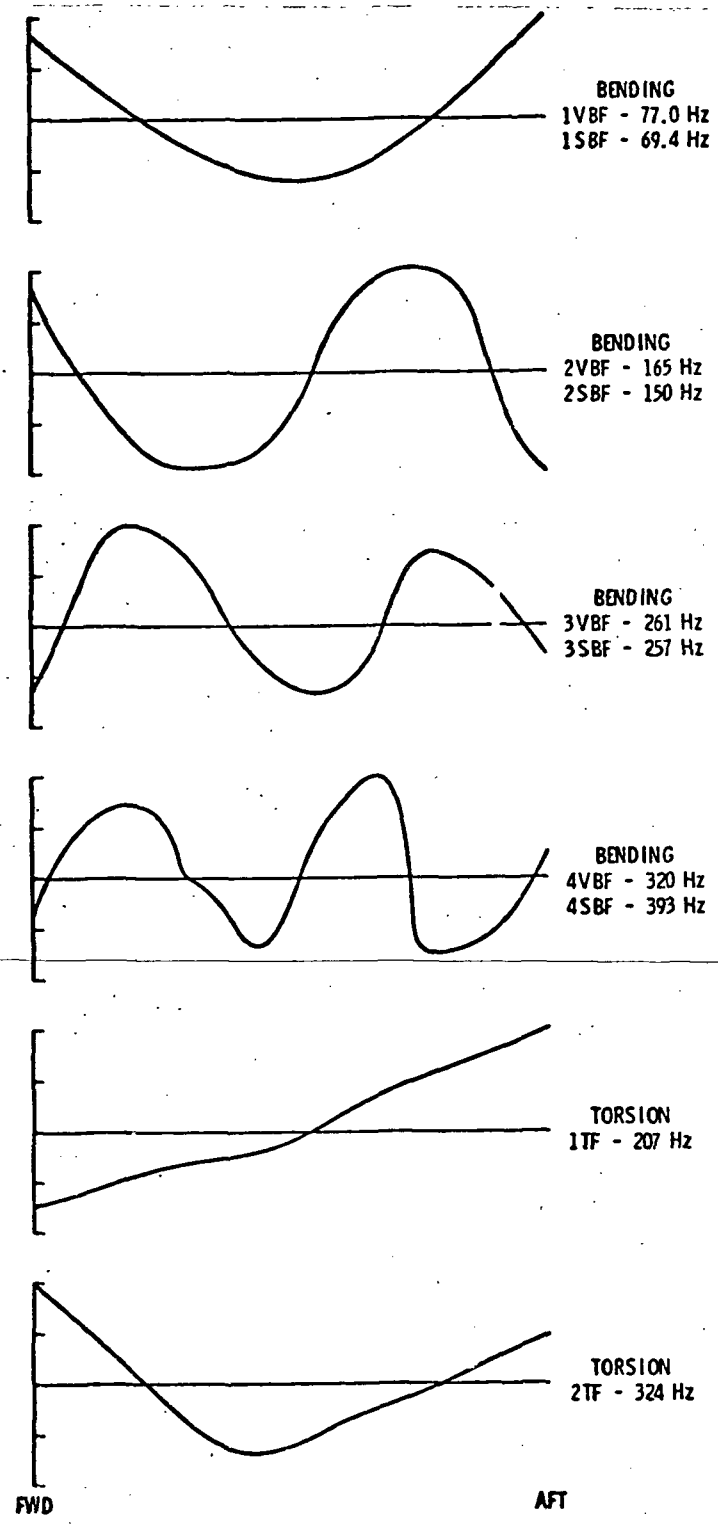

Figure 4a. Component Modes for Free-Free Suspension - H/O Tank

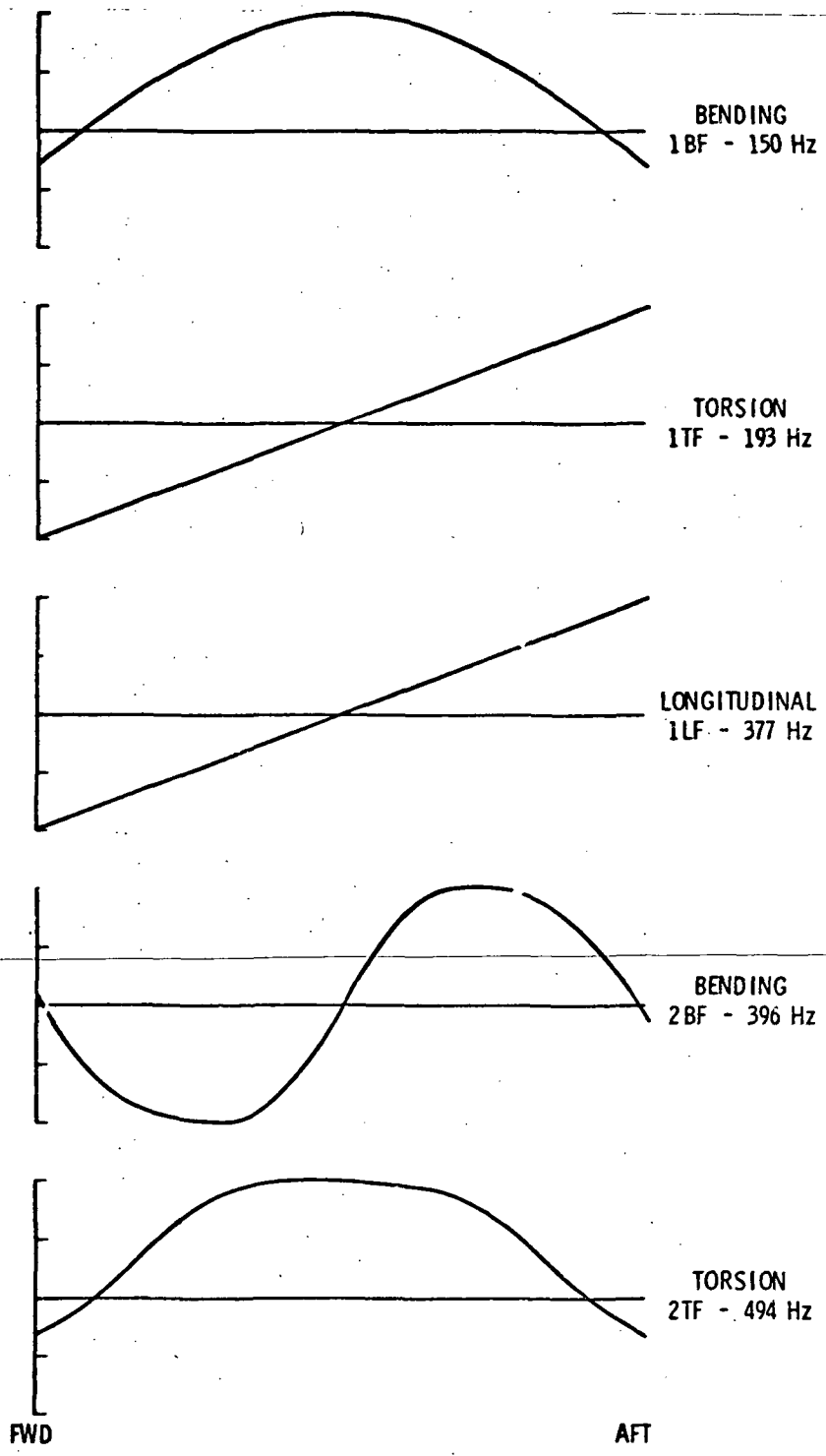

Figure 4b. Component Modes for Free-Free Suspension - Orbiter

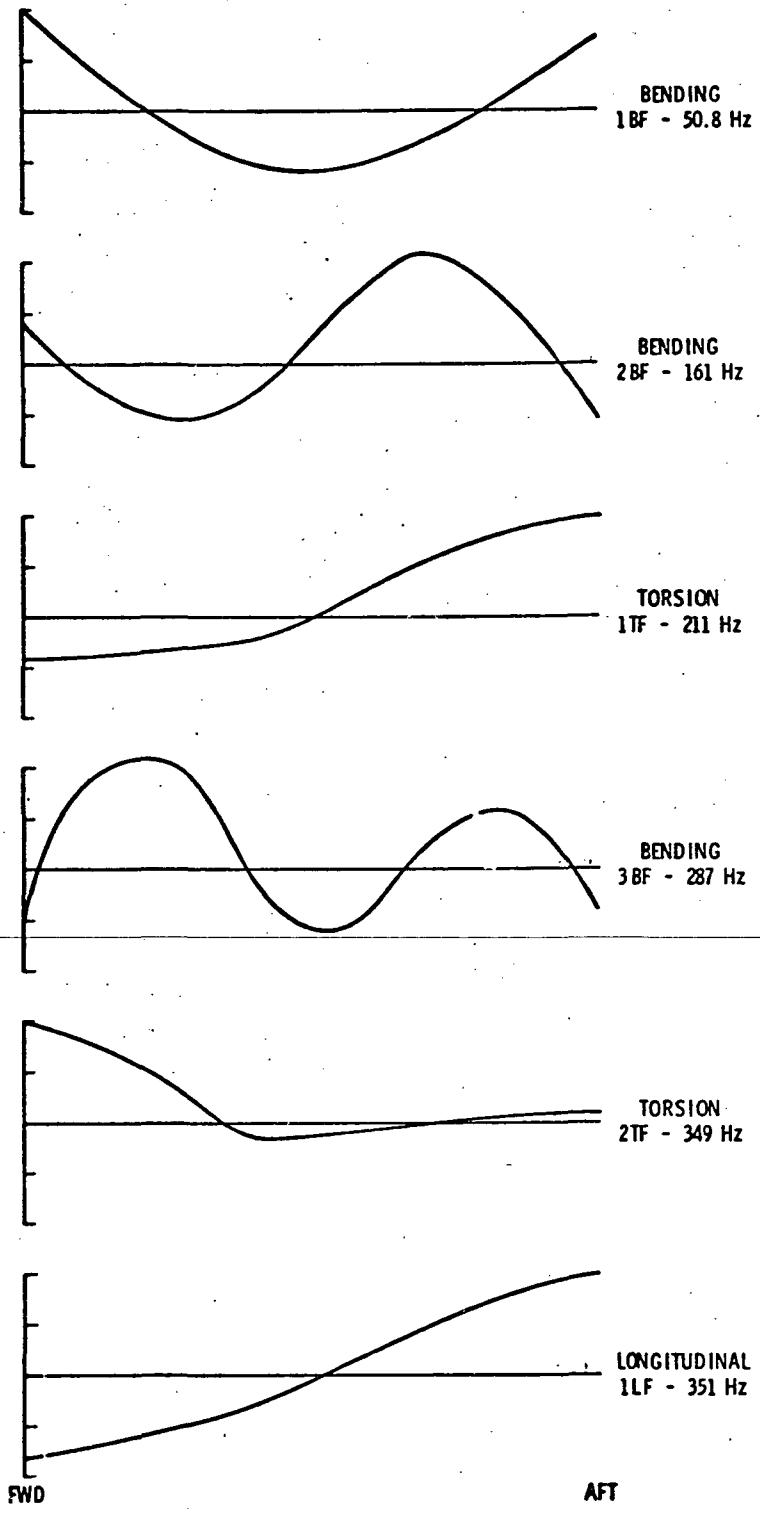

Figure 4c. Component Modes for Free-Free Suspension - Solid Rocket Motors

TABLE II. COMPONENT FREQUENCIES AND DAMPING FOR FREE-FREE SUSPENSION

A. H/O Tank

Mode Identification	Theoretical Frequency Hz	Experimental Frequency Hz	Experimental Damping Ratio
1SBF	69.4	68.4	0.00394
1VBF	77.0	79.8	0.00276
1LQF	96.7	95.0	0.00718
2SBF	150	169	0.00370
2VBF	165	159	0.00362
2LQF	170	186	0.00680
1TF	207	--	--
3LQF	232	238	0.01100
3SBF	257	274	0.00462
3VBF	261	264	0.00466
4VBF	320	--	--
2TF	324	--	--
4SBF	393	435	0.00525
4LSF	394	365	0.00276

B. Orbiter

1BF	150	148	0.0142
1TF	193	192	0.0153
1LF	377	386	0.0162
2BF	396	394	0.0168
2TF	494	--	--
3BF	642	646	0.0172
4BF	703	739	0.0200
3TF	801	--	--
2LF	967	897	0.0179

VB - Vertical Bending
SB - Side Bending
LQ - Longitudinal Liquid
LS - Longitudinal Structure
T - Torsion

TABLE II. COMPONENT FREQUENCIES AND DAMPING FOR FREE-FREE SUSPENSION (Cont'd)

C. Port SRM

Mode Identification	Theoretical Frequency Hz	Experimental Frequency Hz	Experimental Damping Ratio
1BF	50.8	50.0	0.0110
2BF	161	163	0.0136
1TF	211	203	0.0154
3BF	287	298	0.0158
2TF	349	--	--
1LF	351	350	0.0166
4BF	405	432	0.0182
2LF	588	584	0.0190
5BF	597	--	--

D. Starboard SRM

1BF	50.8	50.6	0.0112
2BF	161	164	0.0145
1TF	211	205	0.0162
3BF	287	296	0.0163
2TF	349	--	--
1LF	351	355	0.0170
4BF	405	437	0.0186
2LF	588	595	0.0187
5BF	597	--	--

VB - Vertical Bending
SB - Side Bending
L - Longitudinal
T - Torsion

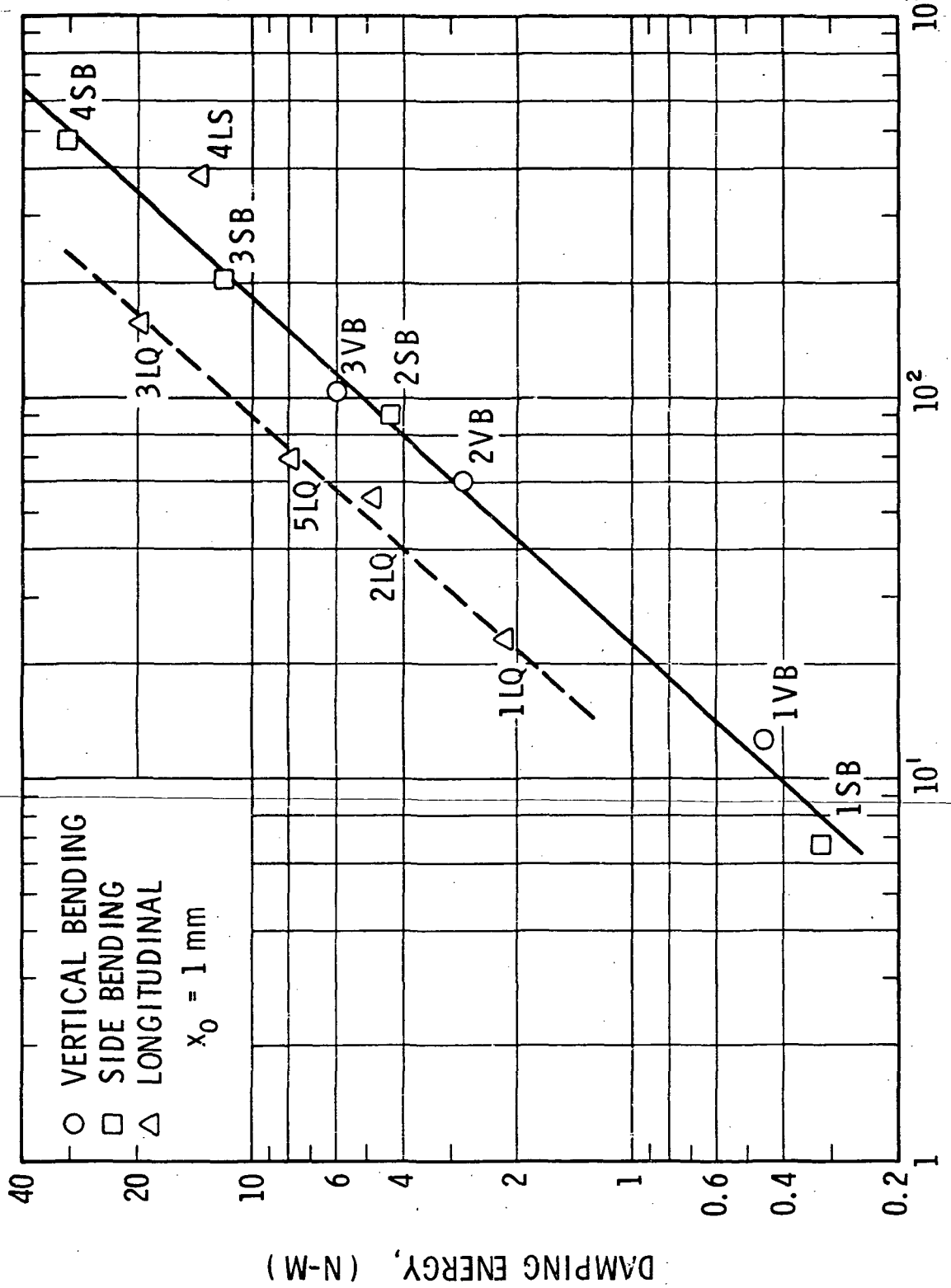

Figure 5. Experimental Damping Energy for H/O Tank

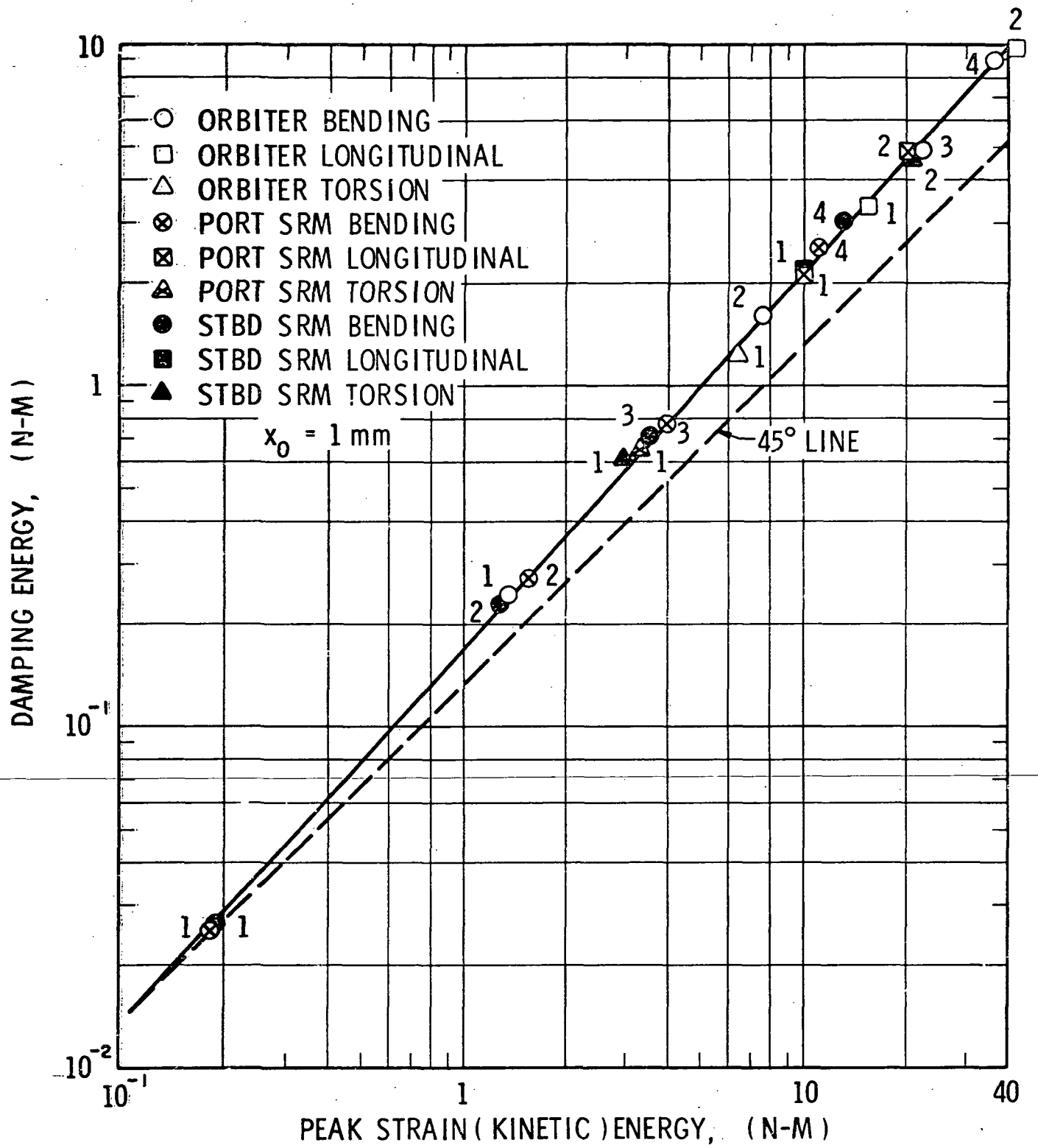

Figure 6. Experimental Damping Energy for Orbiter and Solid Rocket Motors

B. Connecting Links

Damping energy data for connecting links is presented in Figure 7. Although only a few data points are available, a correlation similar to that for the major components is effected. In this case, however, the numbers at each data point correspond to the frequency of a given mode of the connecting link apparatus. The types of modes were also qualitatively identified, but no correspondence with the analytical model was possible because of the type of model postulated. Therefore, these mode shapes will not be discussed.

It can be seen that one test was performed also on a single flexure, and was found to fall near the same correlation line when the energy data were doubled to allow for two springs. Even so, some scatter in the data does occur. At this point it must be admitted that these are the weakest results of the entire study, and will carry into some errors in damping predictions for the lower modes later.

Finally, it can be noted that only a single point is present for the 3-D pin joint, since only one vertical mode could be excited with the procedure utilized. This point fell within the scatter of the correlation line for the flexure joints. As a result, at first we considered using the same correlation line for the damping of vertical motion of the 3-D pins. However, upon further reflection, we used the indicated 45° correlation line, since such a line represents constant specific damping (damping ratio) in the range where no other modes were present. Damping for motion in lateral and longitudinal directions was neglected at the pivot. Again, it is admitted that a more detailed investigation of the joints would have been appropriate, and in fact, was attempted. However, no further useful information was obtained during the time available.

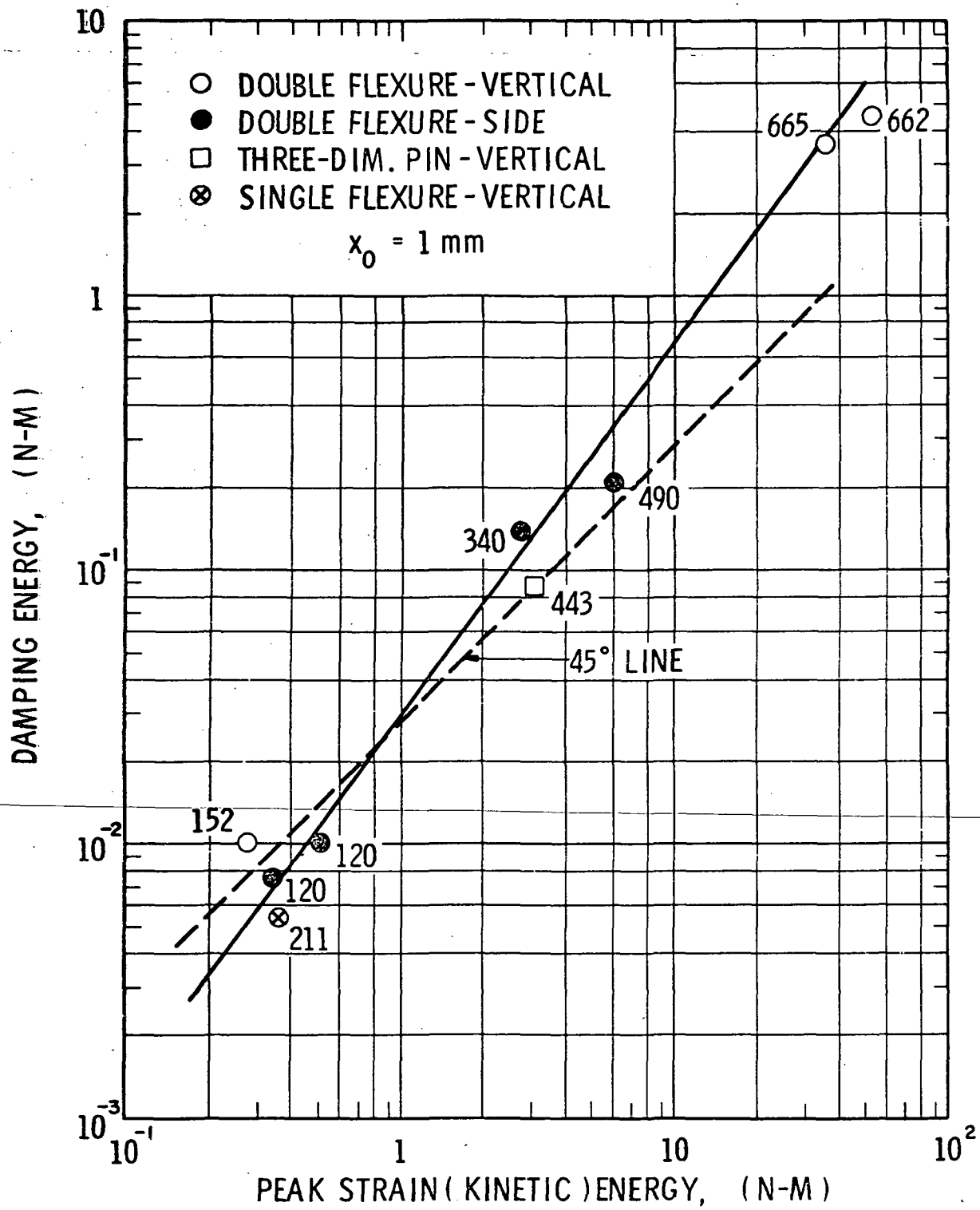

Figure 7. Experimental Damping Energy for Connecting Links

VI. METHOD OF DAMPING PREDICTION

The basic energy method of damping prediction used for this study is essentially the same as that formulated in detail in Reference 2. However, in this case one modification is necessary. In order to be realistic, no damping forces relative to ground are included in the model. As a result, purely rigid body motion of the components relative to the spring supports contribute no damping energy to the system modes (the spring supports themselves do, of course), but do contribute to kinetic energy of the system modes. Thus, it is postulated that only component elastic, or strain energy, is the appropriate parameter to consider for the present application, rather than modal kinetic energy. For freely supported component testing, these two parameters are equal, as has been noted in Figures 5, 6, and 7.

We now will indicate how these curves are used to predict damping for System modes, as summarized in Figure 8. We start with the results from the free vibration eigenvalue problem, which provides system natural frequencies, and corresponding system eigenvectors for all components and connecting links of the system. Within each system eigenvector, of maximum amplitude H, each component experiences a maximum amplitude h_i and each spring support experiences a maximum deflection δ_i, whose values are determined by the system of units used for the analysis.

Step 1. Calculate kinetic energy T_i for each component at amplitude h_i by means of the component eigenvectors and modal mass matrices. Calculate strain energy S_i at amplitude δ_i for all connecting links associated with the i-th component by means of the component eigenvectors and link stiffness matrices. We then can calculate component strain energy at amplitude h_i from

$$U_i = T_i - S_i$$

For those components where the connecting links are not part of the component, $U_i = T_i$. Thus, Step 1 can be eliminated if the connecting links are modeled as separate components themselves.

Step 2. The empirical data of Figures 5, 6, and 7 are in terms of strain energies expressed in metric units, and normalized to X_o = 1 mm maximum amplitude. Therefore, we must convert the above energies by means of

$$\tilde{U}_i = K\,(U_i/h_i^2)$$
$$\tilde{S}_i = K\,(S_i/\delta_i^2) \qquad , \quad X_o = 1 \text{ mm}$$

where K is a constant that provides metric units.

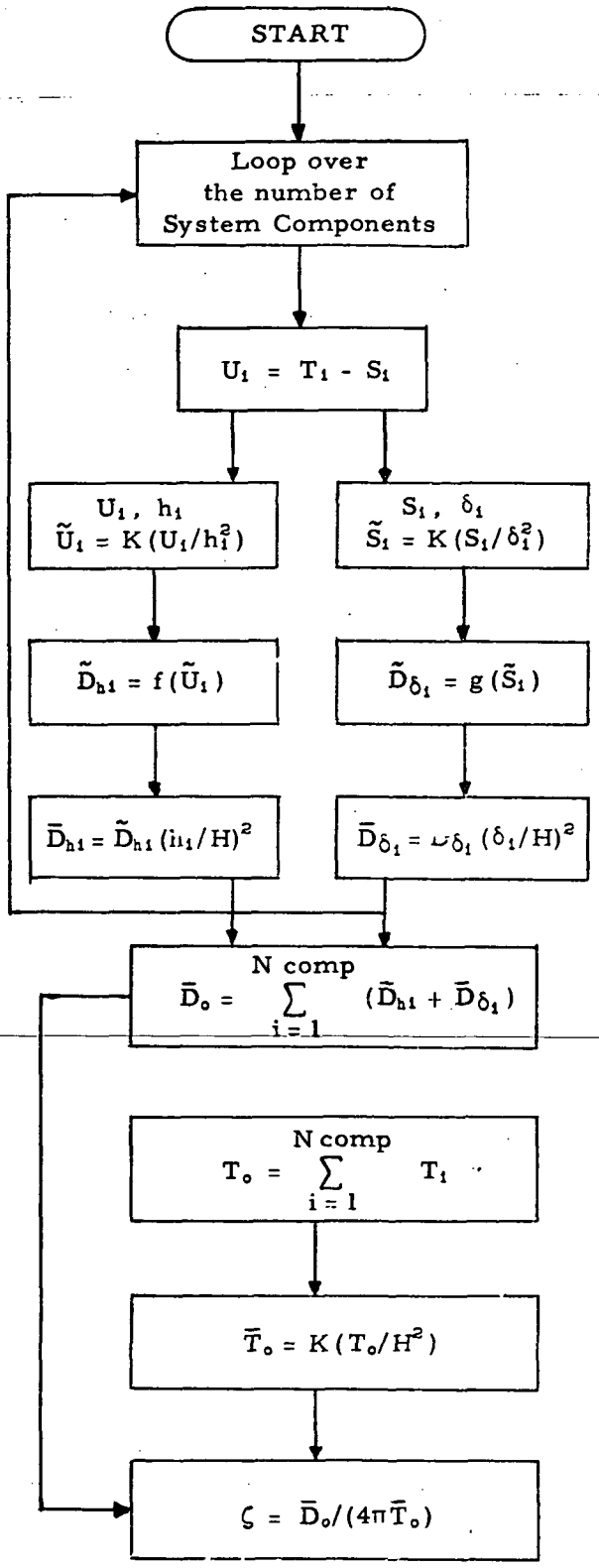

1. Determine strain energy U_i from spring support strain energy S_i and component kinetic energy T_i.
2. Compute strain energy relative to 1.0 mm maximum deflection. K ~ constant for proper units.
3. Determine damping energy from free-free experimental curves, Figures 5, 6, and 7.
4. Compute damping energy relative to 1.0 mm maximum coupled system deflection H.
5. Compute total system damping energy. N comp ~ number of system components
6. Compute system total kinetic energy.
7. Compute system total kinetic energy relative to 1.0 mm maximum coupled system deflection H.
8. Compute modal damping.

Figure 8. Flow Diagram for Damping Calculations

Step 3. The energies of Step 2 are now used to enter the respective curves of Figures 5, 6, and 7. Damping energies $\tilde{D}_{hi}$ and $\tilde{D}_{\delta_i}$, each at $X_o = 1$ mm deflection are obtained from the curves of the form

$$\begin{aligned} \tilde{D}_{hi} &= f(\tilde{U}_i) \\ \tilde{D}_{\delta_i} &= g(\tilde{S}_i) \end{aligned} \quad , \quad X_o = 1 \text{ mm}$$

Step 4. We now adjust the damping energy levels to the proper component and spring amplitudes that occur in a given system mode of maximum amplitude $H = 1$ mm. This is done by the equations

$$\begin{aligned} \bar{D}_{hi} &= \tilde{D}_{hi}(h_i/H)^2 \\ \bar{D}_{\delta_i} &= \tilde{D}_{\delta_i}(\delta_i/H)^2 \end{aligned} \quad , \quad H = 1 \text{ mm}$$

Step 5. Compute the total system damping energy $\bar{D}_o$ for a given mode by summing over all the components and their spring supports:

$$\bar{D}_o = \sum_{i=1}^{N\ comp} (\bar{D}_{hi} + \bar{D}_{\delta_i})$$

Step 6. Compute System total kinetic energy by summing over the kinetic energies of all components:

$$T_o = \sum_{i=1}^{N\ comp} T_i$$

Step 7. Adjust System kinetic energy to $H = 1$ mm maximum modal deflection and convert to metric units.

$$\bar{T}_o = K(T_o/H^2)$$

Step 8. Compute damping ratio for a given System mode from

$$\zeta = \bar{D}_o/(4\pi\bar{T}_o)$$

It must be emphasized that the above procedure includes the assumption of linearity of damping forces with amplitude. However, it also allows for a nonlinear relationship between damping energy and strain energy, as is apparent from Figures 5, 6, and 7.

VII. SPRING-PIN COMPONENT RESULTS

Theoretical data for intermediate Orbiter and SRM modes are given in Figures 9 and 10. These are for components mounted to a rigid wall through their respective connecting links. Again, only those modes within a moderate frequency range are identified. Certain rigid body modes also occur, where the major component acts essentially as a rigid body on the elastic connecting links. The major purpose for these tests was to tune the connecting link compliances of the analytical model to provide the best possible frequency correlation.

A comparison of theoretical and experimental results is shown in Table III. Excellent agreement in frequencies can be seen to have been achieved. As a sidelight, damping ratio predictions were made for this configuration, using the method outlined in Section VI. The results are shown for comparison with measured values. Good agreement was achieved only for the higher mode data. It was found that major discrepancies occurred in the intermediate and lower frequency modes because of significant response occurring in the back-up or support structure that was supposed to simulate a rigid wall. Since this structure would not be present in the total System, it was decided to ignore these discrepancies at this point, and proceed with the investigation of the combined System, rather than redesign the support structure and repeat the intermediate damping tests. It was also felt that significant influence on the frequencies for this configuration was not present. This was substantiated in the System results which will now be discussed.

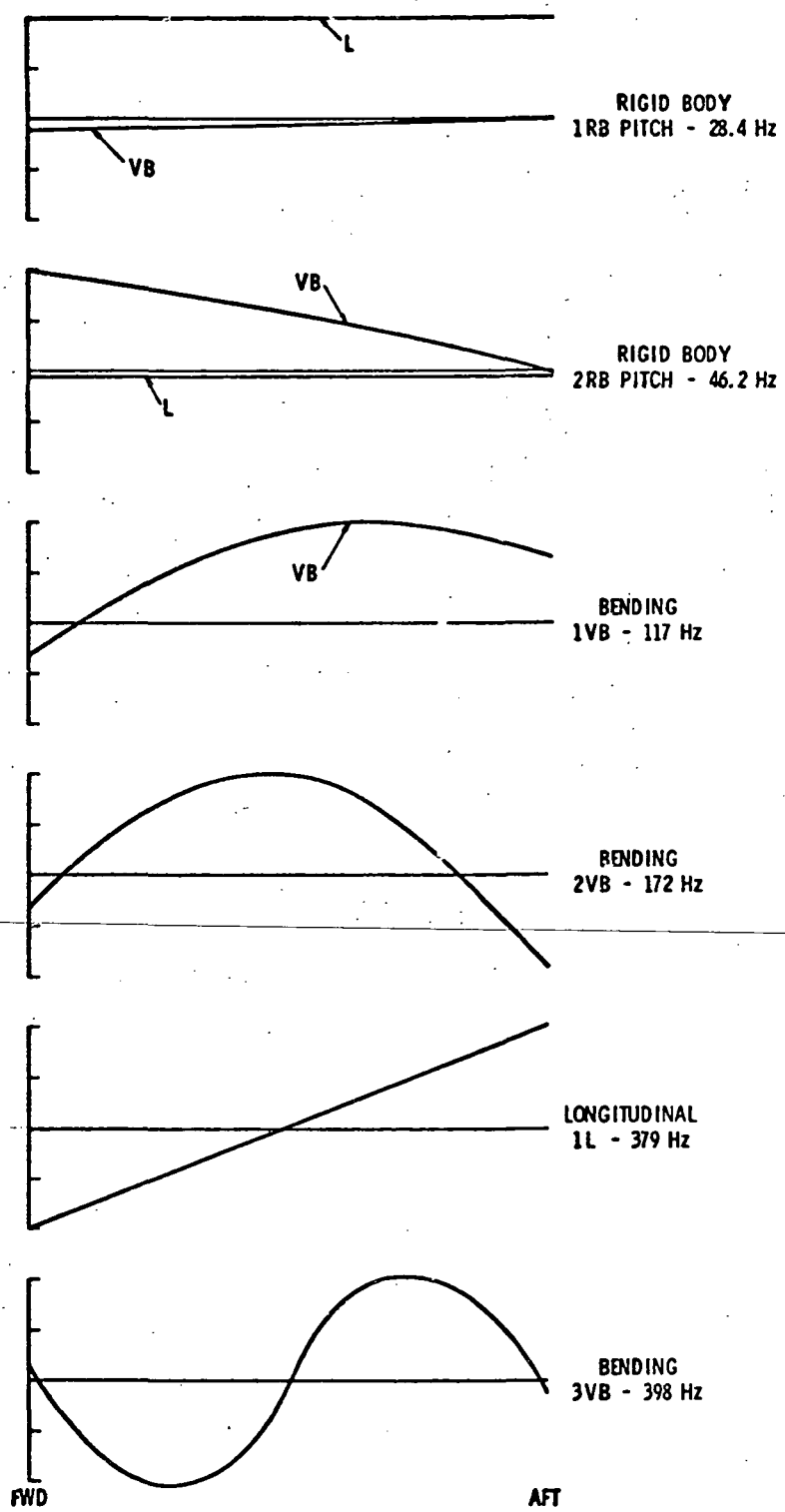

Figure 9a. Orbiter Modes for Spring-Pin Suspension - Symmetric Modes

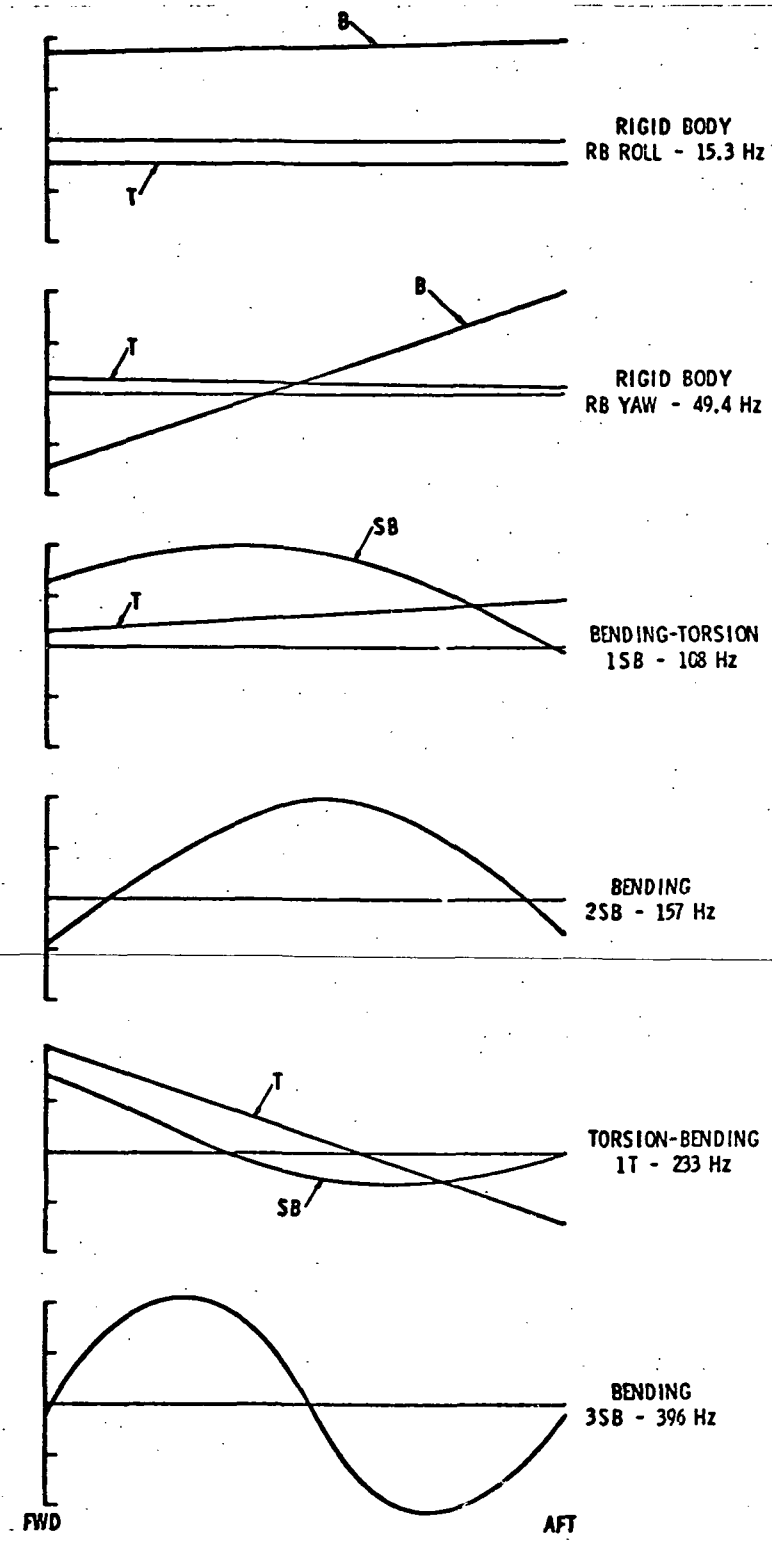

Figure 9b. Orbiter Modes for Spring-Pin Suspension - Antisymmetric Modes

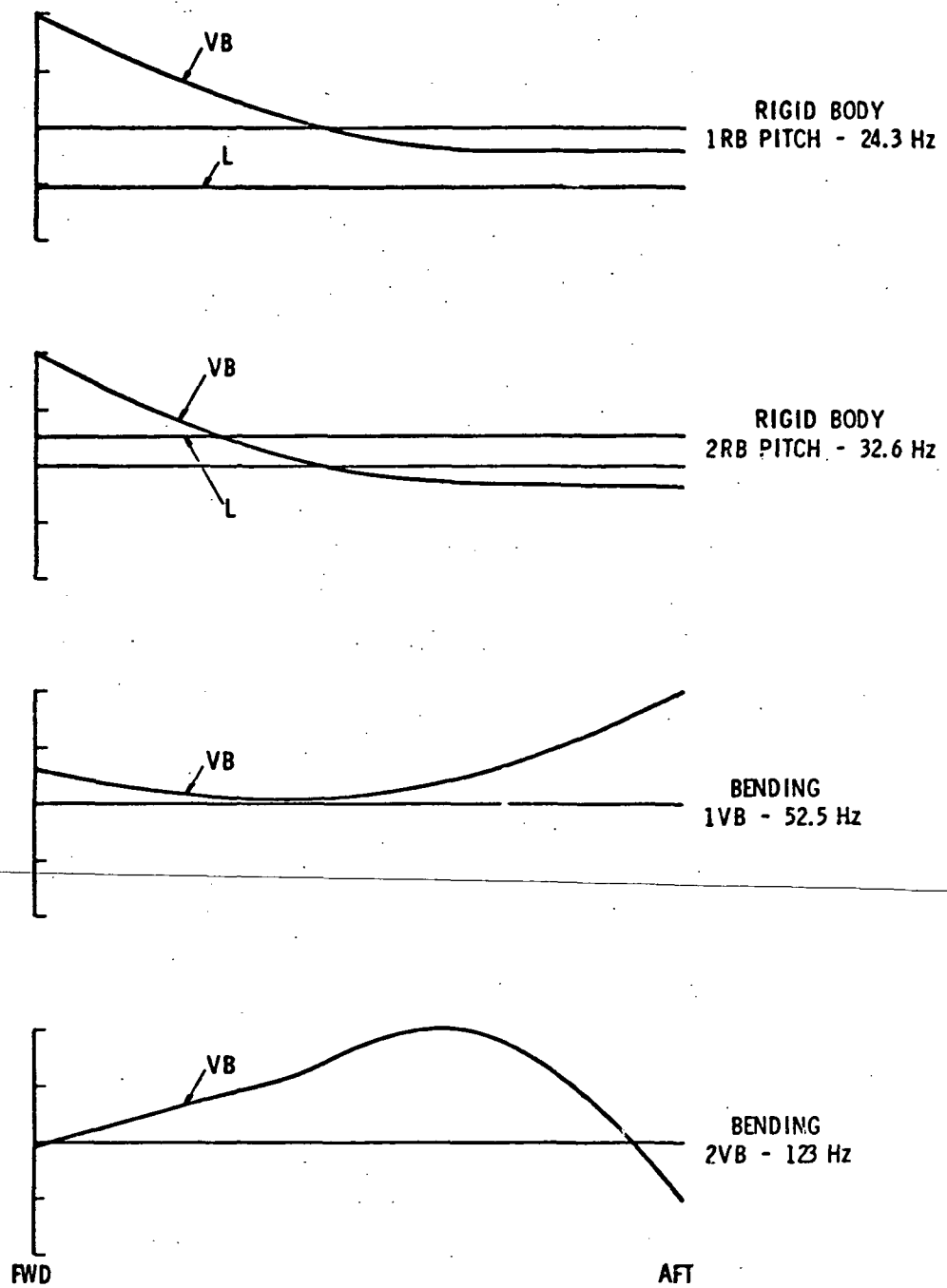

Figure 10a. Solid Rocket Motor Modes for Spring-Pin Suspension - Symmetric Modes (Coupled Longitudinal and Vertical Bending)

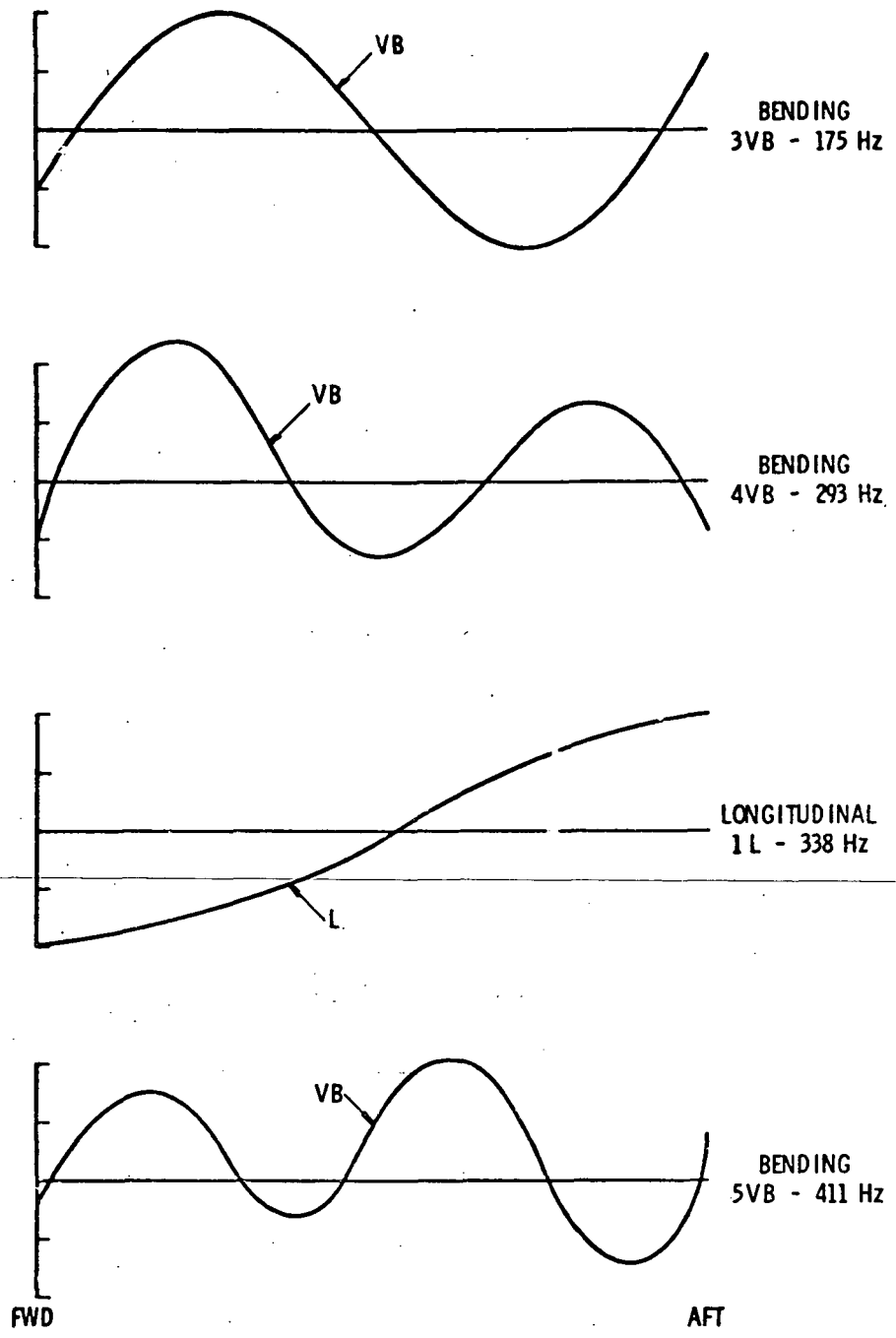

Figure 10a. Solid Rocket Motor Modes for Spring-Pin Suspension - Symmetric Modes (Coupled Longitudinal and Vertical Bending) Cont'd.

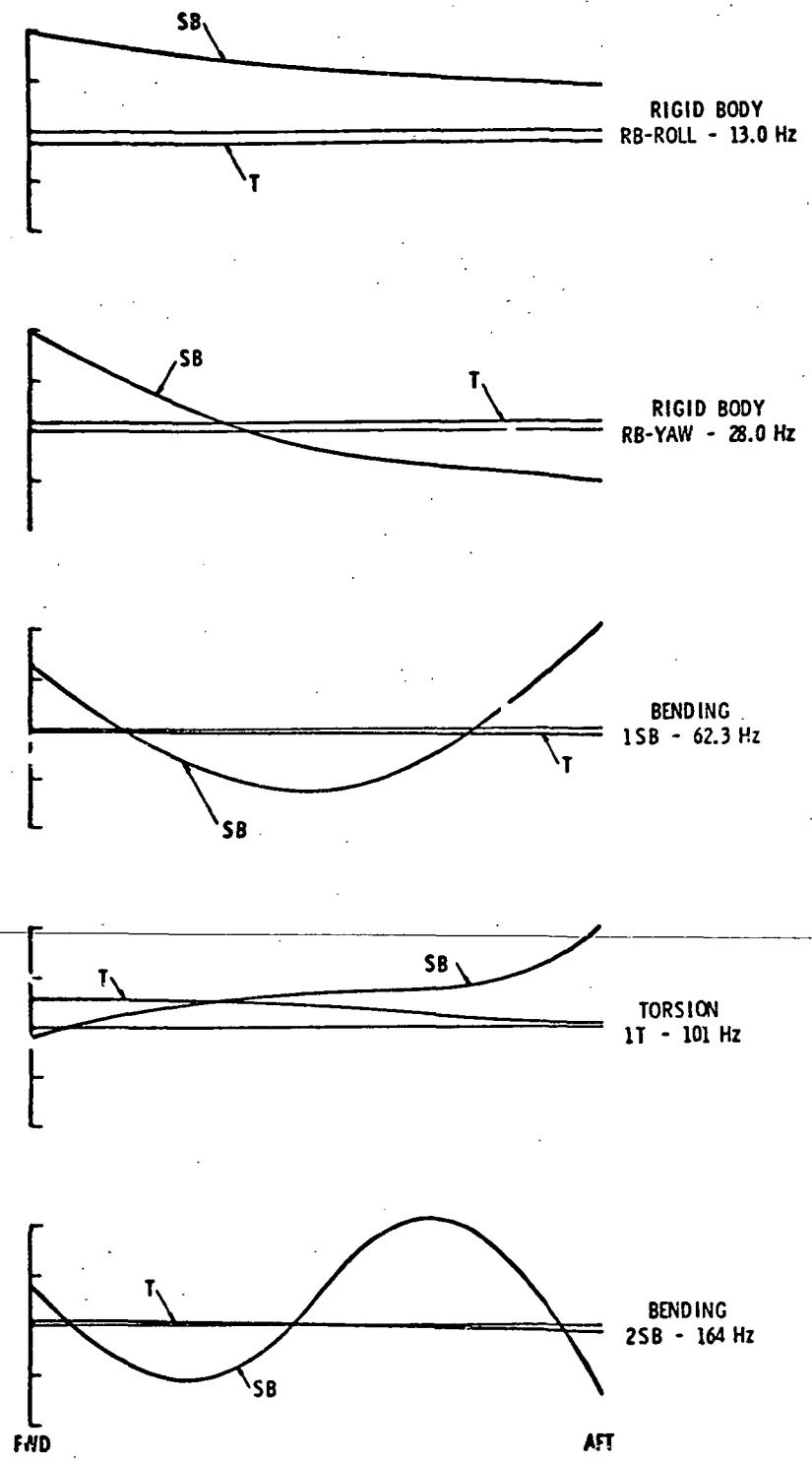

Figure 10b. Solid Rocket Motor Modes for Spring-Pin Suspension - Antisymmetric Modes (Coupled Torsion and Side Bending)

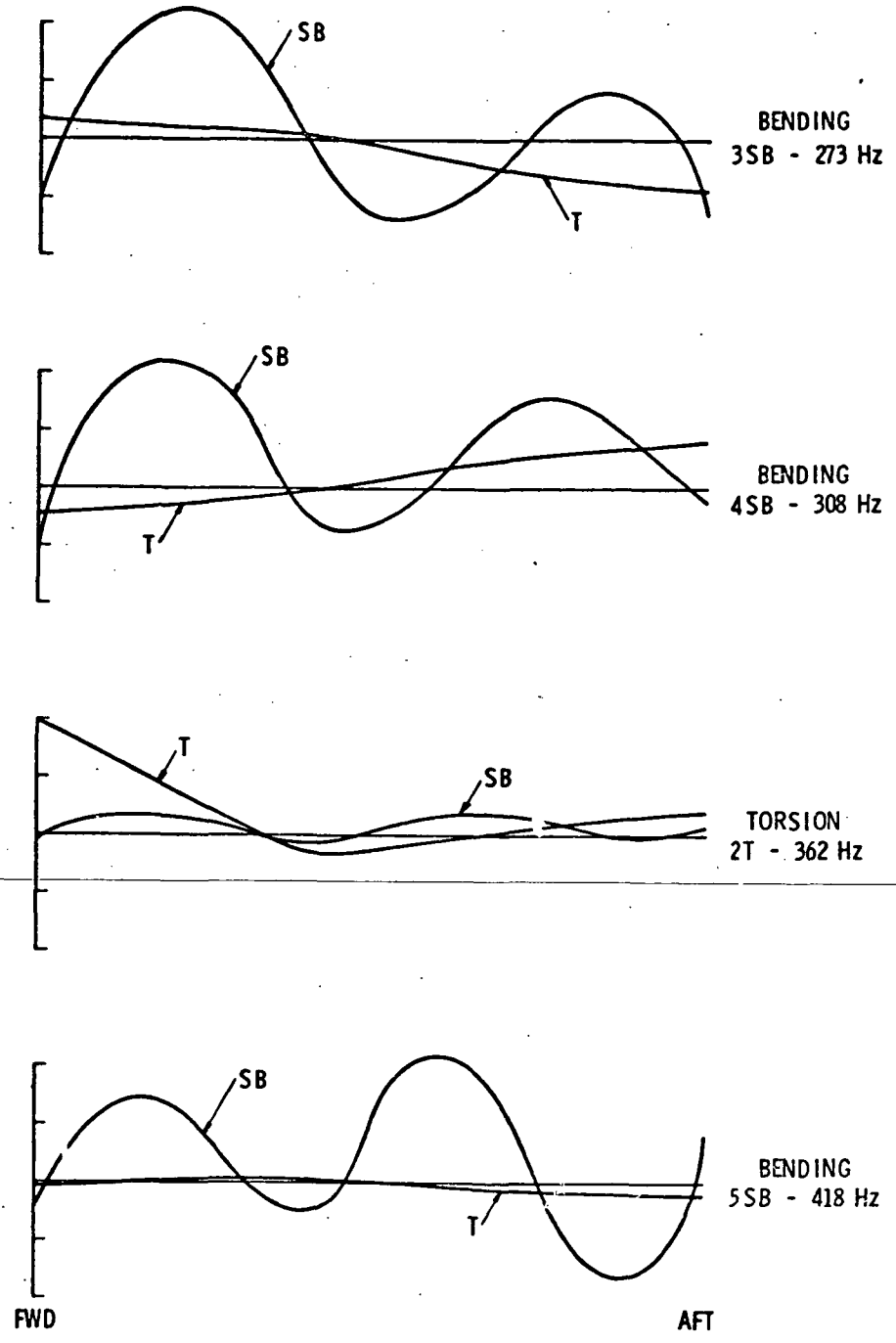

Figure 10b. Solid Rocket Motor Modes for Spring-Pin Suspension - Antisymmetric Modes (Coupled Torsion and Side Bending) Cont'd.

TABLE III. COMPONENT FREQUENCIES AND DAMPING FOR SPRING-PIN SUSPENSION

A. Orbiter

Mode Identification	Theoretical Frequency Hz	Experimental Frequency Hz	Predicted Damping Ratio	Experimental Damping Ratio
RB-roll	15.3	15.6	0.00171	0.00184
1RB-pitch	28.4	28.8	0.00114	0.00439
2RB-pitch	46.2	45.5	0.00142	0.00400
RB-yaw	49.4	49.6	0.00169	0.00560
1SB	108.	101.	0.00666	0.00332
1VB	117.	121.	0.00538	0.0102
2SB	157.	160.	0.0119	0.0143
2VB	172.	178.	0.00936	0.00955
1T	233.	229.	0.0103	0.0090
1L	379.	388.	0.0160	0.0166
3SB	396.	397.	0.0172	0.0167
3VB	398.	346.	0.0179	0.0174

B. Solid Rocket Motors

	Predicted		Experimental Port		Experimental Starboard	
Mode Identification	Frequency Hz	Damping Ratio	Frequency Hz	Damping Ratio	Frequency Hz	Damping Ratio
RB-roll	13.0	0.00234	13.6	0.00164† 0.00245	13.1	0.00178
1RB-pitch	24.3	0.00245	24.7	0.00264† 0.00413	25.7	0.00363
RB-yaw	28.	0.00452	28.9	0.00520	28.7	0.00568
2RB-pitch	32.6	0.00361	30.3	0.00536	35.1	0.00494
1VB	52.5	0.00365	52.9	0.00483	53.5	0.00581
1SB	62.3	0.00645	63.0	0.00790† 0.00869	62.5	0.00745
1T	101.	0.00675	102.	0.0136	100.	0.0106
2VB	123.	0.00684	124.	0.0148	119.	0.0147
2SB	164.	0.0131	168.	0.0139	169.	0.0138
3VB	175.	0.0104	179.	0.0113	179.	0.0116
3SB	273.	0.0134	271.	0.0141	282.	B
4VB	293.	0.0134	304.	0.0153	307.	0.0158
4SB	308.	0.0116	310.	0.0155† 0.0185	314.	0.0138
1L	338.	0.0161	348.	0.0164	350.	0.0160
2T	362.	0.0156	--	--	360.	0.0159
5VB	411.	0.0153	438.	0.0165	--	--
5SB	418.	--	446.	0.0162† 0.0186	442.	0.0183

B ~ Beating

† ~ Double Values Indicate Nonlinearity Range

VIII. COMBINED SYSTEM RESULTS

Theoretical results for all modes within a 400-Hz frequency range are presented in Tables IVA and IVB. The identification of the modes refers back to the basic modal identification presented in Figures 9 and 10 for the intermediate spring-pin configurations for the Orbiter and SRM's, and in Figure 4a for the free-free configuration of the H/O Tank. Of course, because of coupling, the exact shape of the combined modes is different in many cases.

Since the data represent modes of a relatively complex three-dimensional structure, rather than try to depict mode shapes in some type of isometric view, it was decided to describe the modes in terms of the fractional part of the total kinetic energy that was present in each type of motion in each component. In this regard, it must be recalled (see Figure 3) that vertical and side motion of the SRM's are designated relative to their respective mounting springs, and neither of these axis are parallel to the vertical and side axes of the Orbiter and H/O Tank. Also, the modes are designated as symmetric and antisymmetric relative to a plane which passes through the centerlines of the Orbiter and H/O Tank.

The real meat of this entire study is now presented in Table V for the modes which have just been described. Frequency and damping comparisons are presented. Frequency results are seen to be remarkable for so wide a range and number and variety of modes present. Damping results overall are in good agreement, but need considerable discussion. Predicted damping values are given for those which include energy dissipated within the major components (structures) alone, and also for the total which includes that predicted to be dissipated within the connecting links. Of course, the total figure is that which must be compared with the measured values, although joint dissipation affects the lower modes principally.

In general, it can be seen that significant discrepancies in damping exist for some of the lower modes where connecting link damping is dominant. This reflects that a good modeling and, for that matter, damping energy correlation (Figure 7) has not been achieved. However, except for a few isolated cases, better agreement has been achieved for those modes where major component structural response, rather than connecting line response is dominant. Thus, a good damping correlation (Figures 5 and 6) has been achieved in this regard, and the damping prediction method has been validated within reasonable limits.

TABLE IV. THEORETICAL FREQUENCIES AND KINETIC ENERGY DISTRIBUTION

A. Symmetric Modes

Mode Identification	Theoretical Frequency Hz	H/O Longitudinal Motion	H/O Vertical Motion	ORB Vertical Motion	SRM Vertical* Motion	SRM Side* Motion
Roll/SRM	13.9	0	0.109	0.010	0.002	0.879
Pitch/SRM	25.7	0.042	0	0.229	0.726	0.003
Roll/SRM	28.9	0.034	0.026	0.312	0.107	0.521
Roll/SRM & Pitch/ORB	30.1	0.028	0.153	0.299	0.199	0.321
Pitch/SRM	35.3	0.222	0.004	0.070	0.703	0.001
Pitch/ORB	47.4	0.003	0.052	0.914	0.016	0.015
1VB/SRM	52.8	0	0.013	0.012	0.973	0.002
1SB/SRM	60.0	0	0.151	0.021	0.002	0.826
1VB/HO	75.7	0	0.604	0.166	0.011	0.219
1LQ/HO	97.2	0.998	0	0.002	0	0
1T/SRM	103.	0	0.049	0.126	0.001	0.824
2VB/SRM	123.	0	0.045	0.056	0.899	0
1VB/ORB	132.	0	0.326	0.564	0.081	0.029
2VB/HO	162.	0.012	0.463	0.307	0.027	0.191
2SB/SRM	164.	0.007	0.062	0.119	0.004	0.808
2LQ/HO	171.	0.967	0.008	0.006	0.018	0.001
2VB/SRM	175.	0.014	0.019	0.017	0.950	0
VB/HO-ORB	190.	0	0.462	0.496	0.003	0.039
3LQ/HO	233.	1.00	0	0	0	0
3VB/HO	262.	0	0.937	0.002	0.001	0.060
3SB/SRM	275.	0	0.066	0.001	0	0.933
4VB/SRM	293.	0	0.002	0	0.998	0
4SB/SRM	310.	0	0.112	0	0	0.888
4VB/HO	322.	0	0.918	0.001	0.001	0.080
1L/SRM	337.	0	0	0	1.000	0
2T/SRM	353.	0	0.005	0	0	0.995
1L/ORB	379.	0.002	0	0.998	0	0
4LS/HO	394.	0.951	0	0.049	0	0
3VB/ORB	399.	0.048	0.001	0.951	0	0
5VB/SRM	411.	0	0	0	1.00	0

*Both Port and Starboard SRM included.

TABLE IV. THEORETICAL FREQUENCIES AND KINETIC ENERGY DISTRIBUTION (Cont'd)

B. Antisymmetric Modes

Mode Identification	Theoretical Frequency Hz	H/O Longitudinal Motion	H/O Side Motion	ORB Side Motion	SRM Vertical* Motion	SRM Side* Motion
Roll/ORB-SRM	14.7	0.011	0.029	0.582	0.014	0.364
Yaw/SRM	25.3	0.209	0.003	0.132	0.038	0.618
Pitch/SRM	26.9	0.044	0.162	0.025	0.748	0.021
Yaw/SRM	29.4	0.248	0.026	0.093	0.023	0.610
Pitch/SRM	31.7	0	0.051	0.001	0.946	0.002
Yaw/ORB	47.5	0.003	0.131	0.835	0.024	0.007
1VB/SRM	54.7	0.001	0.168	0.013	0.818	0
1SB/SRM	61.6	0.002	0.004	0.010	0.003	0.981
1SB/HO	75.7	0.001	0.724	0.078	0.175	0.022
1T/SRM	103.	0.043	0.015	0.346	0.010	0.586
1SB/ORB	117.	0.191	0.143	0.464	0.028	0.174
2VB/SRM	123.	0.030	0.278	0.064	0.597	0.031
2SB/ORB	155.	0.003	0.208	0.636	0.152	0
2B/HO-ORB-SRM	162.	0.012	0.293	0.346	0.302	0.047
2SB/SRM	163.	0.014	0.013	0.014	0.014	0.945
3VB/SRM	183.	0.002	0.315	0.019	0.664	0
1T/HO	213.	0.748	0.004	0.061	0	0.187
1T/ORB	234.	0.076	0.031	0.886	0	0.007
3SB/HO	259.	0.001	0.982	0.007	0.006	0.004
3SB/SRM	277.	0.065	0.004	0	0	0.931
4VB/SRM	291.	0.001	0.210	0.001	0.788	0
SB/HO	301.	0.009	0.767	0.005	0.219	0
4SB/SRM	310.	0.296	0.005	0.005	0	0.694
1L/SRM	337.	0.001	0	0	0.999	0
2T/HO	338.	0.682	0.006	0.009	0.001	0.302
2T/SRM	355.	0.086	0.001	0.001	0	0.912
4SB/HO	394.	0	0.996	0.003	0.001	0
3SB/ORB	396.	0	0.003	0.997	0	0
5VB/SRM	411.	0	0.004	0	0.996	0

*Both Port and Starboard SRM included.

TABLE V. SYSTEM FREQUENCIES AND DAMPING

A. Symmetric Modes

Mode Identification	Theoretical Frequency Hz	Experimental Frequency Hz	Predicted Damping Ratio (Structure)	Predicted Damping Ratio (Total)	Experimental Damping Ratio	Damping Error Percent
Roll/SRM	13.9	14.6	0.000253	0.000740	0.00179	310
Pitch/SRM	25.7	28.9	0.00288	0.00324	0.00420†	(23
					0.00651	50)
Roll/SRM	28.9	--	0.00310	0.00329	--	
Roll/SRM & Pitch/ORB	30.1	--	0.00298	0.00324	--	
Pitch/ORB	35.3	38.2	0.00104	0.00128	0.00353	64
Pitch/ORB	47.4	46.4	0.00014	0.00128	0.00081	58
1VB/SRM	52.8	55.8	0.00260	0.00356	0.00365 B	2
1SB/SRM	60.0	63.0	0.00667	0.00670	0.00720	7
1VB/HO	75.7	81.7	0.00324	0.00349	0.00327	7
1LQ/HO	97.2	96.7	0.00703	0.00703	0.00500†	(40
					0.00650	8)
1T/SRM	103.	116.	0.00580	0.00679	0.00539†	(26
					0.00660	3)
2VB/SRM	123.	130.	0.00429	0.00696	0.00779†	(11
					0.0110	37)
1VB/ORB	132.	135.	0.00449	0.00570	B	
2VB/HO	162.	160.	0.00746	0.00760	0.00420†	(81
					0.00646	18)
2SB/SRM	164.	165/170.*	0.01208	0.01208	0.00561	115
2LQ/HO	171.	187.	0.00661	0.00661	0.00399†	(66
					0.00595	11)
3VB/SRM	175.	188.	0.00872	0.00970	0.00616†	(57
					0.00770	26)
VB/HO-ORB	190.	198.	0.00159	0.00368	0.00489	(25
					0.00604	39)
3LQ/HO	233.	237.	0.00802	0.00802	--	
3VB/HO	262.	267.	0.00418	0.00418	0.00325†	(29
					0.00417	0)
3SB/SRM	275.	283.	0.0124	0.0124	B	
4VB/SRM	293.	305.	0.0134	0.0134	0.0156	14
4SB/SRM	310.	305.	0.00942	0.0106	0.0111	5
4VB/HO	322.	--	0.00427	0.00442	--	
1L/SRM	337.	349.	0.0161	0.0161	0.0161	0
2T/SRM	353.	357.	0.0153	0.0153	0.161 B	5
1L/ORB	379.	388.	0.0160	0.0160	0.163 B	2
4LS/HO	394.	366.	0.00966	0.00966	0.00177†	(445
					0.00329	194)
3VB/ORB	399.	400.	0.0163	0.0163	0.0174	6
5VB/SRM	411.	431.	0.0154	0.0154	B	

* ~ Mixed Modes
B ~ Beating
† ~ Double Values Indicate Nonlinearity Range

TABLE V. SYSTEM FREQUENCIES AND DAMPING (Cont'd)

B. Antisymmetric Modes

Mode Identification	Theoretical Frequency Hz	Experimental Frequency Hz	Predicted Damping Ratio (Structure)	Predicted Damping Ratio (Total)	Experimental Damping Ratio	Damping Error Percent
Roll/ORB-SRM	14.7	15.3	0.00101	0.00163	0.00101	61
Yaw/SRM	25.3	--	0.00321	0.00349	--	
Pitch/SRM	26.9	25.6	0.00079	0.00105	--	
Yaw/SRM	29.4	32.1*	0.000557	0.00145	0.00135†	(7
					0.00197	26)
Pitch/SRM	31.7	30.8*	0.00384	0.00424	0.00335	27
Yaw/ORB	47.5	50.2	0.00640	0.00640	0.00277	131
1VB/SRM	54.7	53.6	0.00325	0.00394	0.00308	28
1SB/SRM	61.6	65.1	0.00676	0.00676	0.00712	5
1SB/HO	75.7	74.2	0.00209	0.00233	0.00349	33
1T/SRM	103.	116.	0.00490	0.00595	0.00539†	(10
					0.00660	10)
1SB/ORB	117.	108.	0.00335	0.00449	0.00488	8
2VB/SRM	123.	130.	0.00362	0.00537	0.00779†	(31
					0.0110	51)
2SB/ORB	155.	--	0.0103	0.0104	--	
2B/HO-ORB-SRM	162.	169.	0.00797	0.00811	B	
2SB/SRM	163.	--	0.0120	0.0120	--	
3VB/SRM	183.	180.	0.00452	0.00610	0.00710 B	14
1T/HO	213.	--	0.00456	0.00456	--	
1T/ORB	234.	230.	0.00810	0.00910	0.00840 B	8
3SB/HO	259.	261.	0.00373	0.00373	0.00333	12
3SB/SRM	277.	--	0.0125	0.0125	B	
4VB/SRM	291.	305.**	0.0120	0.0120	0.0156	23
SB/HO	301.	--	0.00614	0.00614	--	
4SB/SRM	310.	305.**	0.0114	0.0114	0.0111	3
1L/SRM	337.	349.	0.0162	0.0162	0.0161	0
2T/HO	338.	326.	0.00673	0.00673	B	
2T/SRM	355.	357.	0.0153	0.0153	0.0161 B	5
4SB/HO	394.	--	0.00384	0.00384	--	
3SB/ORB	396.	399.	0.0171	0.0171	0.0165	4
5VB/SRM	411.	431.	0.0154	0.0154	B	

* Mixed Modes

** Influenced by Exciter Location

† Double Values Indicate Nonlinearity Range

The few isolated discrepancies that can be found at the higher frequencies were found to be a result of some anomaly in the modal response. In some cases, a mixing of symmetric and nonsymmetric modes occurred, and in others a distortion in mode shape from that predicted theoretically. Likewise, in some cases data could not be obtained because of beating between modes, or a loss of a weak mode within a nearby more dominant mode. The sources of damping nonlinearity with amplitude were not identified, although were noted to exist for some modes. Finally, some errors may have been caused by the postulation of identical prediction models for the SRM's. Referring back to Table III, one can see that some differences in both frequencies and damping occurred for the pin-spring tests. This probably was a major cause of beating, nonlinearities, and mixing of modes in the combined System.

A special comment is appropriate about the large error that occurred for the fourth longitudinal mode of the H/O Tank (4LS/HO at 394 Hz in Table VA). The predicted damping is somewhat over twice the measured value, even for the upper end of the indicated nonlinear range. By referring back to Figure 5, it can be seen that in the free H/O tank, the corresponding mode (4LS) fell below the correlation line by about a factor of two. This probably means that a third correlation line for longitudinal structural modes alone would be established, if additional higher modes had been obtained. If this were so, then the 0.00966 damping value in Table VA would be more like 0.00483, which would correlate far better with maximum experimental value of 0.00329.

In view of the above comments, a final conclusion is in order with regard to the types of damping energy correlations that can be expected from typical built-up construction that will be present in prototype Shuttle components. It appears from Figure 6 that single-line correlation for all kinds of modes occurs only for a component whose strain energy is absorbed within a structure of uniform or homogeneous material. Such a case is the exception, rather than the rule in typical aerospace construction. It should be expected that multiple correlation curves, such as occurred in Figure 5, will be typical of aerospace structures. Thus, it may occur that individual correlation lines will be found for each type of mode (i.e., bending, longitudinal structure, longitudinal liquid, propellant slosh, etc.). This result is still completely amenable to the energy approach to damping prediction in the combined system, so long as the energy components of the coupled modes are properly identified.

IX. FINAL DISCUSSION

Various comments and explanations of the results have already been given in the preceding sections. Therefore, this final discussion will take the form of recommendations for additional work. No significance is given to the order of presentation.

The major discrepancies of damping prediction found by this study were caused by a lack of adequate definition of the damping characteristics of the connecting links. This part of the work should be revised to provide a better idea of the kinds of testing that will be required to produce reliable results in a prototype system. This should include a retest of all connecting links and a revision of their analytical model representation. It might even be appropriate to consider several different connecting link arrangements.

Additional configurations should be studied. This should include additional liquid levels for the complete System, and a study of the H/O and Orbiter combined together without SRM's, also with various liquid levels. These configurations are also, of course, of equal practical significance.

Some consideration should be given to a remodel of the two SRM's to allow for slightly different frequencies and damping. However, this may or may not allow a more accurate prediction of damping since such anomalies as beating, mixed modes, and distorted modes still cannot be explained by this modification.

Experiments should be conducted whereby accurate measurements of mode shapes are accomplished. This should be done in particular for those modes where discrepancies in damping occurred. Damping prediction is particularly sensitive to variations in mode shape. Measurement of modal kinetic energies for the System at the same time provides another measure of modal discrepancy. This was not done within the present study principally because of a lack of sufficient resources.

The influence of lateral fuel slosh on the dynamic response has not been considered at all. It would be appropriate to redesign the connecting links to lower the system frequencies to where significant coupling with sloshing modes occurs. Then, similar predictions should be made and tested to determine whether damping of lateral liquid propellant motion also falls within the framework of the energy method for damping prediction. The major question is whether a suitable initial correlation can be achieved.

The discovery that a single-line damping correlation apparently can be achieved for sufficiently uniform structures of identical material, but different geometry, is particularly exciting from a fundamental design point of view. The validity of this assertion should be further established both theoretically and experimentally. The result would be the establishment of a single damping energy correlation line for a given material, that could be used to predict damping for all modes of any structural component (i.e., beams, shells, plates) made of that material, regardless of geometry, thickness, boundary conditions, etc.

Finally, it should be asserted that in spite of the indicated remaining uncertainties, it is felt that a good overall validity of the energy method of damping prediction has been demonstrated for a representative Shuttle model. The remaining uncertainties point to the degree of exactness required in the application in order to arrive at useful data, rather than an indication of inapplicability to a prototype Shuttle system. Further application of the method to an even more representative model, such as the scale model being designed and built at NASA Langley Research Center, is very much in order.

REFERENCES

1. Proceedings of Symposium on Substructure Testing and Synthesis, NASA Space Shuttle Dynamics and Aeroelasticity Working Group Meeting, Marshall Space Flight Center, August 30, 1972.

2. Kana, D. D., and Huzar, S., "Synthesis of Shuttle Vehicle Damping Using Substructure Test Results," Interim Report, Contract No. NAS8-27569, Southwest Research Institute, June 1972.

3. Kana, D. D., and Nagy, A., "An Experimental Determination of the Longitudinal Modes of a Simulated Launch Vehicle Dynamic Model," Interim Report, Contract No. NAS8-30167, Southwest Research Institute, March 1970.

4. Glaser, R. F., "Longitudinal Mass-Spring Modeling of Launch Vehicles," NASA TN D-5371, August 1969.

5. Bernhart, W. D., "Computer Program MI 445 for Coupled Vibration Analysis," Memorandum Report 21370, Beech Aircraft Corporation, December 2, 1968.

ACKNOWLEDGEMENTS

The authors wish to express their sincere appreciation to several people who aided in the conduct of this program. Mr. Guido E. Ransleben performed most of the design of mechanical apparatus; and Messrs. Dennis C. Scheidt, George W. Downey, Jr., and Forrest S. Campbell performed the experiments. Special mention should also be given to Mr. Richard W. Schock and Dr. John Admire of Marshall Space Flight Center, who, as Technical Monitors, provided numerous useful suggestions that aided in the successful completion of this program.